REPORT DOCUMENTATION PAGE

FORM APPROVED
OMB No. 0704-0188

1. AGENCY USE ONLY *(Leave blank)*	2. REPORT DATE	3. REPORT TYPE AND DATES COVERED
	September 1997	Final Report 4/1994-6/1997

4. TITLE AND SUBTITLE

A Fundamental Study of Compressibility Effects on Dynamic Stall of Fixed and Adaptive Airfoils

5. FUNDING NUMBERS

ARO-MIPR-133-94

6. AUTHOR(S)

M.S. Chandrasekhara

7. PERFORMING ORGANIZATION NAME(S) AND ADDRESS(ES)

Navy-NASA Joint Institute of Aeronautics. Code AA/CH
Dept. of Aeronautics and Astronautics
Naval Postgraduate School, Monterey, CA 93943

8. PERFORMING ORGANIZATION REPORT NUMBER

9. SPONSORING/MONITORING AGENCY NAME(S) AND ADDRESS(ES)

U. S. Army Research Office
P.O. Box 12211
Research Triangle Park, NC 27709-2211

10. SPONSORING/MONITORING AGENCY REPORT NUMBER

ARO 32480.12-EG

11. SUPPLEMENTARY NOTES

The view, opinions and/or findings contained in this report are those of the author(s) and should not be construed as an official Department of the Army position, policy, or decision, unless so designated by other documentation.

12a. DISTRIBUTION/AVAILABILITY STATEMENT

Approved for public release; distribution unlimited.

12b. DISTRIBUTION CODE

13. ABSTRACT *(Maximum 200 words)*

A three year research effort on "A Fundamental Study of Compressibility Effects on Dynamic Stall of Fixed and Adaptive Airfoils" was initiated in 1994. The research led to an understanding of: some of the key mechanisms of compressible dynamic stall including when the flow over the airfoil is transonic; the Reynolds number effects which strongly alter the detailed flow physics making extension of laboratory results to full-scale conditions extremely challenging, and the role of transition and a need to model it properly in computations. Further, the results demonstrated the major role of the airfoil leading edge curvature in producing the flow gradients that are responsible for dynamic stall onset, which enabled the development of a dynamically developing leading edge (DDLE) airfoil for effective flow control by modifying the vorticity field in the flow. The significant results of the effort are summarized in this report.

14. SUBJECT TERMS

Compressible Dynamic Stall Mechanisms, Reynolds Number Effects, Adaptive Flows Geometry

15. NUMBER OF PAGES

44

16. PRICE CODE

17. SECURITY CLASSIFICATION OF REPORT	18. SECURITY CLASSIFICATION OF THIS PAGE	19. SECURITY CLASSIFICATION OF ABSTRACT	20. LIMITATION OF ABSTRACT
UNCLASSIFIED	UNCLASSIFIED	UNCLASSIFIED	UL

A FUNDAMENTAL STUDY OF COMPRESSIBILITY EFFECTS ON DYNAMIC STALL OF FIXED AND ADAPTIVE AIRFOILS

FINAL REPORT

M.S.CHANDRASEKHARA

SEPTEMBER 8, 1997

U. S. ARMY RESEARCH OFFICE

ARO CONTRACT NUMBER: 32480-EG

DEPARTMENT OF AERONAUTICS AND ASTRONAUTICS
NAVAL POSTGRADUATE SCHOOL
MONTEREY,CA 93943

FINAL REPORT

A Fundamental Study of Compressibility Effects on Dynamic Stall of Fixed and Adaptive Airfoils

1. FOREWORD

A three year research effort on "A Fundamental Study of Compressibility Effects on Dynamic Stall of Fixed and Adaptive Airfoils" was initiated in 1994. The research led to an understanding of: some of the key mechanisms of compressible dynamic stall including when the flow over the airfoil is transonic, the Reynolds number effects which strongly alter the detailed flow physics making extension of laboratory results to full-scale conditions extremely challenging, and the role of transition and a need to model it properly in computations. Further, the results demonstrated the major role of airfoil leading edge curvature in producing the flow gradients that are responsible for dynamic stall onset, which enabled the development of a dynamically developing leading edge(DDLE) airfoil for effective flow control by modifying the vorticity field in the flow. The significant results of the effort are summarized in this report.

Funding support received through MIPRs ARO-133-94, ARO-110-95, ARO-96-7 and MIPR7CNPSARO12 to the Naval Postgraduate School(NPS) is gratefully acknowledged. During the reporting period Mr. Robert D. Van Dyken was awarded Ph.D. from NPS for his work on the compressible dynamic stall problem. This experimental study was conducted in the Fluid Mechanics Laboratory(FML) of NASA Ames Research Center. The support of the Branch Chief, Dr. S.S.Davis, the cooperative participation of Dr. L.W.Carr, Group Leader, Unsteady Viscous Group, U.S. Army AvRDEC & ATCOM are sincerely appreciated.

2. TABLE OF CONTENTS

3. LIST OF FIGURES

(a) Untripped, (b) Tripped

Fig. 18. Global Pressure Coefficient Distribution, M = 0.45, k = 0.05, $\alpha = 10^0$

Fig. 19. DDLE Shape Profiles Compared with the NACA 0012 Profile

Fig. 20. Flow Modification with Changing Leading Edge Shape, M = 0.3, k = 0.0, $\alpha = 18.00^0$. (a) Shape 0, (b) Shape 9, (c) Shape 13, (d) Shape 17

Fig. 21. Flow Regimes for Different Leading Edge Shapes *vs.* Angle of Attack, k = 0.0, (a) M = 0.3, (b) M = 0.45

Fig. 22. Vorticity Flux Distributions for DDLE Shapes 0, 4, 8, 10, M = 0.3, k = 0.0, (a) $\alpha = 12.03^0$, (b) $\alpha = 13.99^0$, (c) $\alpha = 18.00^0$

Fig. 23. PDI Images and Corresponding Global Pressure Distributions for Oscillating DDLE Shape 8 Airfoil, M = 0.3, k = 0.05, $\alpha = 10^0 - 10^0 \sin\omega t$

4.A. STATEMENT OF PROBLEM STUDIED

It is now well known that compressibility promotes dynamic stall onset to progressively lower angles of attack as the freestream Mach number is increased. Increasing Reynolds number has a slight benefit in this regard. However, since laboratory tests are conducted on rotors at model-scale conditions, the extension of such test results to full-scale rotor Reynolds numbers has remained an art. There is also the effect of freestream turbulence (or the rotor-blade wake-turbulence) which seems to promote transition onset on the blade section whose effects are still not properly understood. Computational modeling of the flow has not satisfactorily included the role of transition in altering the dynamic stall process, resulting in significant discrepancies with experimental data. The modeling of transition in deep dynamic stall flow is indeed a very challenging task.

The differing stall onset mechanisms even for slightly varying model-scale flow conditions in the transonic regime add further complexities to this problem. As a consequence, controlling dynamic stall has proved very difficult. The present study was aimed at primarily understanding the fundamental fluid flow physics of compressible dynamic stall flow at widely differing flow conditions ranging from Mach number (0.2 -0.45), Reynolds number ($0.54 \times 10^6 - 1.6 \times 10^6$ where a laminar separation bubble plays a major role), reduced frequency (0 - 0.1) and oscillation amplitude (2 deg and 10 deg), with and without a boundary layer trip on a 6-inch chord NACA 0012 airfoil. This phase of the study led to the identification three different mechanisms of compressible dynamic stall. Also, after establishing that the flow gradients near the leading edge (the source of much of the unsteady vorticity in the dynamic stall flow) need to be manipulated for effective control, a novel concept was developed for dynamic stall control. It involved the use of a dynamically deforming leading edge (DDLE) for a basic NACA 0012 airfoil whose leading edge curvature could then be varied in real-time by a large value to introduce dramatic changes in the local flow. Preliminary tests were carried out on an oscillating DDLE airfoil to demonstrate the concept.

4.A.1. Nomenclature

C_p pressure coefficient

$C_{p_{min}}$	peak pressure coefficient
c	airfoil chord
f	frequency of oscillation, Hz
k	reduced frequency $= \frac{\pi f c}{U_\infty}$
L	test section span
M	freestream Mach number
U_∞	freestream velocity
x,y	chordwise and vertical distance
α	angle of attack
α_0	mean angle of attack
α_m	amplitude of oscillation
ϵ	fringe number
ρ	density
ρ_0	density at atmospheric conditions
ρ_r	density at reference conditions
ϕ	phase angle of oscillation
ω	circular frequency, radians/sec

4.A.2. Description of the Experiment

The experiments were carried out in the the compressible dynamic stall facility(CDSF) located in the Fluid Mechanics Laboratory(FML) of NASA Ames Research Center. NASA and FML provided much of the instrumentation and material needed for the research. The nonintrusive optical flow measurement technique of Point Diffraction Interferometry(PDI) was used in the study. A description of the facility, DDLE airfoil design and the measurement technique is given below.

4.A.2.1. The Compressible Dynamic Stall Facility

The CDSF is an indraft wind tunnel with a 10 in X 14 in test section and is equipped with a drive for producing sinusoidal variation of the airfoil angle of attack. The flow in the tunnel is controlled by a computer driven, choked, variable area downstream-throat, to

obtain a Mach number range of $0.1 \leq M \leq 0.5$. The flow is produced by a 6MW, 240,000 CFM, continuously running evacuation compressor. The airfoil mean angle of attack can be set to $0 \leq \alpha \leq 15^0$, the amplitude of oscillation to $2^0 \leq \alpha_0 \leq 10^0$, and the oscillation frequency to $0 \leq f \leq 100Hz$. In the studies to be reported, a 6-inch chord NACA 0012 was supported between optical glass inserts in metal ports in the tunnel side walls. Optical access from the stagnation point at high angles of attack to the first 35% chord on the airfoil upper surface was available with this model mounting arrangement.

4.A.2.2. The Dynamically Deforming Leading Edge Airfoil

Earlier studies (Ref. 1) have clearly demonstrated the role of the leading edge adverse pressure gradient in inducing compressible dynamic stall. As a result, control of dynamic stall requires modifying this gradient for changing flow conditions. By designing an airfoil whose geometry could be adapted to the instantaneous flow conditions, it may be possible to control compressible dynamic stall. One of the major goals of the study was to establish the hitherto unknown fluid mechanics of flow over such airfoils. Towards this goal, the DDLE airfoil was designed and fabricated. In the particular design developed for this study, the airfoil leading edge curvature could be varied by as much as 320% to produce dramatic flow changes around its leading edge where compressible dynamic stall originates. Such an airfoil was tested for demonstrating the feasibility of achieving flow control.

The philosophy used for the design of the DDLE airfoil was: relative to that of the fixed geometry airfoil,

1. reduce the suction peak pressures at high angles of attack
2. reduce the strong adverse pressure gradient
3. distribute the suction pressure over a wider region of the upper surface in order to improve the airfoil performance.

The major design considerations were: the force required to produce the desired deformation at rapid rates in the unsteady flow under investigation (oscillating airfoil flow at a freestream Mach number of up to 0.45 and frequencies of 20 Hz); the material fatigue properties; the continuity of slope and curvature of the airfoil surfaces; and the fabrication effort required. The airfoil nose curvature was specified to be varied from that of the 6

in chord NACA 0012 airfoil to a fully rounded leading edge airfoil, resulting in a 320% change in curvature (from 0.095 in radius to 0.30 in radius) through a maximum leading edge retraction of 0.08 in. The rate of leading edge movement was required to be programmable, with the fastest deformation rates specified to occur within one-quarter cycle of motion on the airfoil upstroke. After a dwell time at this rounded shape, the leading edge was returned to its original NACA 0012 profile, which was maintained for the rest of the cycle.

Based on these requirements, the final choice was a design consisting of a carbon-fiber composite skin for the airfoil surface from the leading edge up to the 0.2c location; the rest being made from solid metal. The skin was attached with a tang to a mandrel shaped to the leading edge profile of a 6 in chord, NACA 0012 airfoil, housed *inside* the airfoil. Fig. 1 shows these details and Fig. 2 depicts a schematic of the mounting arrangement and drive system in the CDSF.

The mandrel is linked to a truss, which is in turn linked to a drive motor on each end through connecting rods. The DDLE motors are 2.1 hp brushless servo-stepper motors capable of intermittent operations through rapid, short angular motion. The motors are equipped with a 4096 steps/rev resolver with an accuracy of ± 7 arc min. An encoder with 5400 counts/rev is mounted on the motor shaft to provide a digital display of the leading edge position. The motors are software driven from a PC through controllers which provide the ability to hold the DDLE at any predetermined position for as long as required for accomplishing detailed flow studies. It is possible to move the DDLE at different speeds through a range of positions or incrementally in minimum time to obtain a step change of shape. Fig. 3 shows the time history of motion obtained at different rates. It is clear that at the fastest rate, V(10), (where 10 denotes the highest rate parameter used in programming the drive system) the motion was completed in about 15 ms, as designed. There is a minimum rise time of 3 ms in all cases compared. The feed back control is finely tuned to hold the airfoil shape against the wind load and to complete the required movements without introducing jitter during movement or oscillations at the ends of the duty schedule. The full details of DDLE design, fabrication and control system are described in Ref. 2.

A typical motion history consists of pushing the DDLE from a selectable relative home position to the most forward position (the NACA 0012 shape) where it is held until commanded to execute the desired deformation schedule at a pre-determined rate. The motion is phase locked to the desired airfoil angle of attack in its sinusoidal motion cycle as shown in the flow chart in Fig. 4. When a match occurs between the selected and actual angles of attack, a trigger pulse is issued by the Oscillating Airfoil Position Interface(OAPI) to the servomotor controller through a signal conditioner unit. The controller software (which is pre-loaded from the PC) is interrupt driven for phase locking purposes, with the interrupt pulse generated from the OAPI. The movement of the motors and thus of the DDLE is initiated by the controller following this event as shown in Fig. 4. A slightly varying time delay (attributable to ongoing real-time processing within the PID loop) exists in the controller leading to some uncertainty (of the order of a few encoder counts) in phase locking. Presently this problem is being addressed, but success has been achieved by the simple solution of repeating the experiments.

4.A.2.3. Instrumentation and Techniques

As stated earlier, PDI was used in the study to obtain quantitative flow field density information. Its optical arrangement was similar to that of a standard Z-type schlieren system, but the light source was a laser beam expanded (to 15 cm) to fill the field of view of interest in the test section. The optics were aligned to minimize astigmatism. The knife edge was replaced by a pre-developed, but not fixed, (partially transmitting) photographic plate (AGFA 8E75HD). This was necessary to burn an appropriate sized pin-hole in it to serve as the point diffractor and generate the reference beam. Imaging optics were set up further downstream along the beam path for recording the flow as shown in Fig. 5. With no flow in the test section, a pin-hole was created *in situ* in the photographic plate. Light refracted by the flow density changes (signal beam) focused to a slightly different spot overlapping the point diffractor and passed through the partially transmitting photographic plate, interfering with light passing through the pin-hole (which thus becomes the reference beam) to produce interference fringes in real time, which were then recorded on Polaroid film. Ref. 3 fully describes the technique and its implementation

in the CDSF.

4.A.2.4. Interferogram Image Processing

Several hundred interferograms were obtained during the experiment. These were scanned and processed manually using a software package developed in-house. Both surface and global pressure fields have been derived from the interferograms. Also, a nearly automated processing package is now available (Ref. 4) which can trace and provide pixel maps of the fringe centerlines for subsequent interpretation manually.

In the PDI images, it must be noted that increasing positive fringe numbers represent flow deceleration and vice versa. Hence, fringes from the freestream to the stagnation point have positive values, with the freestream fringe having a value of 0. The corresponding pressure along a fringe, up to the boundary layer edge, was derived using isentropic flow relations as:

$$C_p = \frac{\left[\left(\frac{\rho}{\rho_r}\right)^{\gamma} - 1\right]}{\left[\frac{\gamma}{2}M^2\right]}$$

For the specific case of the present experiments,

$$\rho - \rho_r = 0.009421\epsilon$$

or

$$\frac{\rho}{\rho_0} = \frac{\rho_r}{\rho_0} + \frac{0.009421\epsilon}{\rho_0}$$

Since $\frac{\rho_r}{\rho_0}$ is a function of the freestream Mach number only, $\frac{\rho}{\rho_0}$ can be determined by knowing the fringe number. The pressure at the edge of the boundary layer was then used as the surface pressure under the boundary layer assumptions.

4.A.2.5. Experimental Conditions

Most of the experiments were conducted for a flow Mach number range from $0.2 \leq M \leq 0.45$. The corresponding Reynolds number ranged from $0.54 \times 10^6 - 1.6 \times 10^6$. The oscillation frequency was varied from 0 - 45 Hz, resulting in reduced frequencies from 0 - 0.1. The airfoil was oscillated about the 25% chord point, with its angle of attack varying as $\alpha = 10^0 - 10^0 \sin \omega t$. These results were compared with those obtained earlier for the

3-inch chord NACA 0012 airfoil to establish Reynolds number effects at constant Mach number and investigate the different mechanisms of dynamic stall.

To simulate a higher Reynolds number, several different trips were used on the airfoil. The most successful one (as determined by the criteria of delay of stall onset angle, increased suction peaks and thickness comparable to the local boundary layer height, Ref. 1) was made from a 1.5%-chord-long address label, 0.003 in thick located between x/c = 0.005 to 0.02. The tripped airfoil studies were compared with the untripped airfoil flows in both steady and unsteady (10 deg. amplitude) flows, for k = 0.05 and 0.1 at M = 0.3 and for k = 0.05 at M = 0.45.

Preliminary tests were conducted on DDLE airfoil to evaluate the concept for controlling separation. Different shapes were studied over a range of high angles of up to 18 deg at different Mach numbers in steady flow. Subsequently, flow interferograms were obtained for selected shapes while sinusoidally oscillating with angle of attack varying as $\alpha = 10^0 - 10^0 \sin\omega t$ at M = 0.3.

4.A.2.6 Experimental Uncertainties

The uncertainty in C_p depends on the fringe number under consideration and is 1 fringe for the flow in general with about 3 fringes possibly undetectable near the suction peak at M = 0.3. Since correction for solid and wake blockage was less than 5% for $C_p = -6.0$ at M = 0.3, and $\alpha = 12^0$, only uncorrected PDI derived pressures are reported. The losses in the tunnel screens causing a decrease in the stagnation pressure have been included in the computation of the reference density in this otherwise atmospheric flow wind tunnel.

By far the largest uncertainty in C_p appears from the very strong density gradient near the airfoil leading edge which introduces strong refractive index gradients. The effect of this is to deflect the light rays towards higher density regions. Hence, a dark region develops on the upper surface near the leading edge (Ref. 6) in some images. No corrections were applied to the C_p values on this account because of the strong dependence of the beam displacement on the local density gradient which in turn depends on instantaneous angle of attack, freestream Mach number, and reduced frequency. Also, it was found that by

slightly realigning the PDI optics, the distortion could be minimized. With this solution, it was estimated that the true suction peak location was displaced by less than 0.5% of airfoil chord towards the trailing edge. Support for this can be found by directly comparing the pressures measured using surface taps and those obtained with PDI as shown in Fig. 6 (Ref. 7) for the 6-inch airfoil in steady flow at M = 0.3. At α = 8 deg, Fig. 6a, the two agree very well. At α = 13 deg, Fig. 6b, there is agreement to within the one fringe standard uncertainty of the PDI method. The differences seen at the laminar separation bubble location are due to the insufficient number pressure taps over the airfoil that make it impossible to record the pressures at the resolution of PDI.

With these considerations, the estimated uncertainties are as follows:

Mach number:	± 0.005
angle of attack:	0.05 degrees
reduced frequency:	0.005
C_p:	± 0.1 at M = 0.3
$C_{p_{min}}$:	-0.5 at M = 0.3
	-0.45 at M = 0.45
$\frac{dC_p}{d(x/c)}$	± 25

4.B. SUMMARY OF SIGNIFICANT RESULTS

4.B.1. Mechanisms of Compressible Dynamic Stall

4.B.1.1. Laminar Separation Bubble Bursting

It has been shown in Ref. 8 and 9 that for Reynolds numbers $\leq 1 \times 10^6$ and low freestream Mach numbers, (M = 0.3 - 0.35) dynamic stall originates from the bursting of a laminar separation bubble that forms as the airfoil pitches up. Fig. 7 presents three PDI images for the untripped airfoil at M = 0.3 and k = 0.05 where it can be clearly seen to be the case. The fringes run parallel to the surface for a short distance downstream of the suction peak, but turn abruptly towards it to form the bubble for α = 8.98 deg, Fig. 7a. As the leading edge adverse pressure gradient increases, the bubble begins to burst at α = 12.47 deg in Fig. 7b and shortly later in the pitch-up motion, at α = 13.48 deg, Fig.

7c, a well defined imprint of the dynamic stall vortex is observed. Earlier studies reported in Ref. 1 show that the adverse pressure gradient attains a local maximum for this angle of attack. A similar result was obtained for the tripped airfoil which, however, was able to withstand a slightly higher adverse pressure gradient as shown in Fig. 8.

4.B.1.2. Shock-Induced Separation

Interferograms of the flow at M = 0.45 and k = 0.05, Re = 1.6×10^6 that show dramatically different flow details are presented in Fig. 9. Due to the higher Reynolds number of the flow a shorter laminar separation bubble forms, Fig. 9a. More importantly, a supersonic region has already formed at $\alpha = 7.53$ deg here and begins to grow rapidly for even slightly higher angles of attack, Fig. 9b. At $\alpha = 8.4$ deg, this region extends over the bubble and another half-a-degree later, $\alpha = 8.98$ deg, grows in vertical extent over the airfoil as well. For this conditions, a series of compression and expansion waves are present in the flow, which can be attributed to the transonic flow over the convex leading edge curvature of the airfoil, as shown by Guderley (Ref. 10). As seen in Fig, 9d, this region terminates in a shock. A thickening of the boundary layer occurs at the foot of the shock which is more clearly seen in Fig. 9e for $\alpha = 9.49$ deg as the shock induces separation. It is interesting to note here that even though a supersonic region was recorded in the dynamic stall flow over the 3-inch airfoil, none of the multiple shocks observed was strong enough (local upstream Mach number ≥ 1.2) to produce the necessary pressure rise (1.4) across it and thus, the flow remained attached. Supersonic flow exists even downstream of the shock as a supersonic tongue is seen downstream. At $\alpha = 10.72$ deg in Fig. 9f, the dynamic stall vortex has grown to an oval shape as it is constrained by the supersonic flow above it. This is a significantly different imprint of the dynamic stall vortex when compared to the lower Reynolds number flow development where it was found to be nearly circular. It is also interesting to note the very small angle of attack range (about 2 deg) over which so many significant developments occur in the flow. The supersonic region persists until a higher angle of attack and eventually becomes subsonic as the flow expands.

4.B.1.3. Interaction Between Laminar Bubble and Local Supersonic Flow

Even more interesting interactions are observed for intermediate range of Reynolds number and Mach number. The growth of the supersonic flow region and the tendency of the bubble to burst with increasing angle of attack present a situation when complex interactions occur leading to a new source of dynamic stall.

Figure 10a shows a PDI image for an angle of attack of 7.97 deg for M = 0.35, k = 0.05 for the 6-inch untripped airfoil. As before, a laminar separation bubble can be seen in the picture; it ends where the fringes near the leading edge turn abruptly towards the airfoil surface (at $x/c \approx 0.04$). The boundary layer downstream of the bubble is still fairly thin. In Fig. 10b, at an angle of attack of 10.00 deg, the boundary layer begins to thicken at the downstream end of the bubble. The Mach number corresponding to the peak suction pressure now is about 0.92. Soon after, the local flow becomes supersonic. At this instant, the suction peak flow is supersonic, but the bubble is subsonic and the two are separated by some distance. The supersonic region grows more along the airfoil than above it and extends to the bubble by $\alpha = 11.5$ deg, Fig. 10c. A close examination of the local fringe pattern indicates that the fringe denoting the suction peak is absent. Instead, the fringes develop parallel to the airfoil upper surface. The nearly flat fringes imply that the adverse pressure gradient is significantly reduced (see Fig. 11) from that observed for the case of M = 0.3 and k = 0.05 where the flow is subsonic. It should be noted that although the bubble flow is subsonic everywhere, its upstream end is suddenly subjected to a supersonic flow. At this time the boundary layer at the downstream end of the bubble becomes even thicker (a precursor to stall). At the same time, tiny disturbance waves form in the supersonic flow region as the Mach number at the suction peak reaches about 1.05, (see also Fig. 12). These are expansion and compression waves reflecting off the sonic line above the convex leading edge of the airfoil and the shear layer. These unsteady transonic flow waves can cause dramatic variations in pressure along the weak shear layer enclosing the bubble, which could either alter the bubble dynamics by influencing transition and reattachment or simply force separation by preventing reattachment, causing dynamic stall, depending upon their instantaneous strength. If the bubble continues to exist, its

bursting is dictated by the pressure distribution in the supersonic flow unlike that seen for the lower freestream Mach number case where the flow was subsonic everywhere. Whereas dynamic stall eventually ensues, the above described fine scale events compete with each other and play a major role in its onset. Further, it is very difficult to capture these details experimentally. But the effects are easily discernible once stall has begun. In Fig. 10d, at $\alpha = 12.03$ deg, the shear layer at the downstream end of the bubble can be seen to be lifting off the surface as the dynamic stall vortex forms underneath it. Even though shocks are still seen in the flow after the dynamic stall process has begun, flow separation was not attributed to the these, because a fringe count indicated that the maximum local Mach number upstream of the shock was only about 1.1 which is not enough to cause flow separation. Interestingly, the airfoil peak suction increases slightly during further pitch-up of the airfoil. This is because dynamic stall begins at $x/c \approx 0.035$ and until the upstream end of the vortex reaches the leading edge, the peak suction development continues, since there is no propagation of information upstream (except through the separated shear layer) in the local supersonic potential flow. Although a similar result was obtained at $M = 0.3$, the supersonic flow for the case of $M = 0.35$ resulted in a much altered viscous/inviscid interaction.

The distributions of the adverse pressure gradient in the untripped and tripped flow at $M = 0.35$ and $k = 0.05$ are shown in Fig. 11. A dramatic difference can be seen between the two. As stated earlier, the development of the fringes parallel to the airfoil surface after the suction peak results in very low adverse gradients. Yet, dynamic stall occurred by about 11.5 deg. In contrast, if the same airfoil was properly tripped, a very large adverse pressure gradient develops before dynamic stall occurs. Thus, Fig. 10 and 11 clearly illustrate the very different mechanisms of dynamic stall that can occur depending upon changes in local flow conditions.

Fig. 12 shows a similar sequence of events as described above, but for $M = 0.45$ and $k = 0.05$ for the 3-inch untripped airfoil. The higher freestream Mach number means that supersonic velocity is reached at even lower angles of attack, where the bubble is still not subjected to the large adverse pressure gradient. The spread of the supersonic region is more rapid in this case due to the higher initial Mach number and thus, the range of

angles of attack over which the interactions described above occur is smaller, leading to an even earlier dynamic stall onset (by about 9.5 deg). The qualitative similarity between the results presented at the two different Reynolds numbers in Fig. 10 ($\mathrm{Re} = 1.3 \times 10^6$) and Fig. 12 ($\mathrm{Re} = 0.81 \times 10^6$) confirms that compressibility effects drive the major flow events. It is noted that at the same freestream Mach number, the higher Reynolds number flow produces a larger suction peak value and thus, a higher local Mach number. Thus, Reynolds number affects the physics of the problem through the significantly altered viscous/inviscid interactions that are responsible for the development of peak suction, which primarily determines the strength of the supersonic flow and the state of the boundary layer, which in turn determines whether a bubble forms, etc.

These cases provide examples of the situation in which the dynamic stall process could have been caused by the bursting of the bubble if the supersonic flow had not interfered with the shear layer and the bubble, creating competing mechanisms of stall onset. If the local Mach number were slightly higher, shock induced separation would have occurred as described above.

4.B.2. Influence of Reynolds Number

One of the main thrusts of the effort was to document the influence of Reynolds number on dynamic stall process. Also, it was of interest to see whether laboratory results could be extended to full-scale Reynolds number flow situations. Hence, a 6-inch airfoil was tested with and without a trip on it and the data compared with that obtained for a 3-inch airfoil - at the same Mach number. In effect, this provided four data sets at different equivalent Reynolds numbers, but at *one* Mach number. It has been said in Ref. 7 that $\frac{1}{7}^{th}$ scale model-rotor dynamic stall data agree satisfactorily with full-scale Reynolds number oscillating airfoil dynamic stall data and that no other equivalence can be found in the body of data available. It was speculated that some of this was due to the effect of rotor-wake turbulence, based on water tunnel test results of Ref. 11 conducted in a high freestream turbulence tunnel at $\mathrm{Re} = 5 \times 10^4$ that yielded good agreement with the full-scale Reynolds number data of Ref. 12. If so, the question is: is there a minimum Reynolds number at which tests can be conducted where the effects of higher freestream

turbulence, namely promotion of transition onset can be achieved? The present study used boundary layer tripping to simulate this effect.

4.B.2.1. Development of Airfoil Peak Suction at M = 0.3

The development of airfoil peak suction with increasing angle of attack is shown in Fig. 13, where the full-scale Reynolds number (4×10^6) data of Ref. 13 is also included for M = 0.3 and k = 0.05. The increase in peak suction level with increasing Reynolds number is evident here. The drop-off in the suction peak is associated with the onset of dynamic stall and the formation of the dynamic stall vortex. Fig. 13 shows the slight delay in the dynamic stall onset angle to higher values at higher Reynolds numbers. For example, the dynamic stall onset angles are 12.8 deg, 13 deg, 13.5 deg for the untripped 3-inch airfoil, the tripped 3-inch airfoil, the 6-inch untripped airfoil respectively. Interestingly, the angle is 14 deg for both the 6-inch tripped airfoil and for the experiments of Ref. 13. This enables the 6-inch airfoil to continue to generate the higher levels of suction and thus, higher lift at higher Reynolds numbers. For the low Reynolds number cases, the magnitude of the suction peak remains constant over a small angle of attack range when the dynamic stall vortex forms and organizes before convecting. Fig. 13 shows that at higher Reynolds numbers, this phase of the flow is short indicating a more rapid evolution of dynamic stall. In fact, for the 6-inch tripped airfoil and for the 24-inch airfoil of Ref. 13, dynamic stall onset appears as soon as the peak suction reaches its maximum level. Similar results were obtained for the unsteady case of k = 0.1. For the highest two Reynolds numbers (1.1×10^6 and 4×10^6) under discussion, the peak suction pressure reached values that produced locally supersonic flow.

4.B.2.2. Effect of Reduced Frequency at M = 0.3

Figure 14 presents the effect of Reynolds number on the development of suction peak for M = 0.3 and k = 0, 0.05 and 0.1. Fig. 14a for the 3-inch airfoil restates that there is a phase lag in the peak suction development which increases with reduced frequency. The figure also shows that the peak suction increases with reduced frequency. Fig. 14b for the tripped 3-inch airfoil shows the same lag effect, and that tripping increases the

suction levels compared to the corresponding untripped cases. However, in Fig. 14c for the 6-inch untripped airfoil, the peak value is about -7.0 for all three cases, but the noted phase lag is still present. Also, the flow has become slightly supersonic in all these three cases at $Re = 1.1 \times 10^6$. Similar data from Ref. 13 from Fig. 14 shows that the airfoil develops a maximum $C_{p_{min}}$ of about -9.0 for all three cases compared. The increase in $C_{p_{min}}$ with Reynolds number can be attributed to the decreasing viscous effects at the higher Reynolds numbers. While it can be expected that the peak suction would reach the unsteady inviscid value which is even higher than that found in the high Reynolds number experiments ($Re = 4 \times 10^6$) the differences will get smaller as the Reynolds number is increased above this value. Thus, one can conclude that whereas compressibility still dominates the development of dynamic stall for $M \geq 0.3$ at all Reynolds numbers, Reynolds number still plays a major role until a limiting Reynolds number is reached, above which the flow is completely determined by Mach number effects. This interaction between compressibility effects and Reynolds number effects is a significant factor in the evolution of dynamic stall for different conditions.

4.B.2.3. Comparison of Pressure Distributions at M = 0.3, k = 0.05

In an effort to establish if oscillating airfoil data from a test at a lower Reynolds number can be used to represent flight Reynolds number conditions comparisons of the PDI pressure distributions have been made with those in Ref. 13 for M = 0.3 and k = 0.05 over an untripped airfoil. Fig. 15a compares the 6-inch airfoil pressures at 7.97 deg with those of Ref. 13 at 7.88 deg. The untripped 6-inch airfoil distributions exhibit a plateau in the region x/c = 0.02 - 0.05 which corresponds to a laminar separation bubble that is absent in the high Reynolds number data. There is a small difference in the suction peak level, but downstream of the plateau the distributions agree very well. The tripped airfoil nearly reproduces the overall pressure distribution of Ref. 13 at this angle of attack. Any differences seen are within the uncertainty of the PDI data. Fig. 15b shows the data at 10.0 deg for the PDI experiments and 9.97 deg for the reference set. The agreement between the tripped 6-inch airfoil data and the high Reynolds number data is good. A bubble can still be seen in the untripped 6-inch case between x/c = 0.02 – 0.04.

Fig. 15c is drawn for $\alpha = 12.03^0$ which is compared with $\alpha = 12.11^0$ of Ref. 13 data. The laminar separation bubble has shrunk and is now located between approximately $0.015 \leq x/c \leq 0.03$ for the untripped airfoil. For Fig. 15d the data are compared at 12.98 deg and 13.00 deg respectively. In both Figs. 15c and 15d the tripped data includes data points obtained from magnified PDI images of the leading edge flow field. A very good agreement can be seen in the overall pressure distribution with the data at $Re = 4 \times 10^6$. At high angles, near the suction peak some differences appear which are due to the shadow of the trip located near the leading edge. As the peak suction increases with increasing angle of attack, the fringe density becomes very high (about 20-25 dark fringes/mm, i.e. a total of 40-50 black and white fringes in the first 1.5% of the airfoil chord) and it is then comparable to the resolution of the Polaroid film (about 20 lines/mm) used to record the images. It is estimated that as many as 7-8 fringes may have been lost in this dark region due to the high fringe density and inadequate film resolution. If uncertainty due to these factors is included in the comparisons as shown, the two data sets agree quite well everywhere. It should be noted that the problem becomes acute only at high angles of attack. The dynamic stall onset angle of about 14 deg for the tripped 6-inch airfoil test compares well with that obtained in Ref. 13. This agreement is important for dynamic stall control efforts since the the same control scheme has to work in both model and full-scale situations, the model-scale flow has to effectively replicate the physics of the full-scale flow. Good agreement in the pressure distributions and stall onset angle and elimination of the undesirable effects of a laminar separation bubble with a trip enhance the chances of success with flow control.

Similar agreement was obtained for M = 0.3, k = 0.1 flow conditions. Thus, it is believed that the present compressible dynamic stall experiments on a 6-inch tripped airfoil using PDI have successfully reproduced the measurements of Ref. 13.

4.B.2.4. Comparison of Flow Adverse Pressure Gradients

Figure 16 shows the adverse pressure gradient in the flow following the suction peak for the various cases being discussed at M = 0.3 and k = 0.05. Despite the noise inherent in gradient determination, it is clear from Fig. 16 that the untripped 6-inch airfoil flow

can support about 30% higher nondimensional adverse pressure gradient than the 3-inch untripped airfoil flow, even though in both flows laminar separation bubble bursting caused dynamic stall onset. Interestingly, the two data sets overlap from $\alpha = 8^0$ until stall onset in the 3-inch airfoil flow. Also, the tripped flow cases and the high Reynolds number data follow each other in the angle of attack range from 9.0 - 12.0 deg. The tripped 6-inch airfoil flow can withstand a slightly higher pressure gradient than the tripped 3-inch airfoil flow prior to dynamic stall onset. Even though the $Re = 4 \times 10^6$ flow seems to support a very large gradient of about 280, dynamic stall occurred at $\alpha = 14$ deg as it did for the 6-inch tripped airfoil. In general, the ability to withstand higher adverse pressure gradient appears to be the reason for the delay of stall observed with increasing Reynolds number.

4.B.2.5. Effect of Unsteadiness at M= 0.45

Figures 17a and 17b demonstrate the effect of changing reduced frequency from 0, 0.05 and 0.1 for the 6-inch untripped and tripped airfoils at M = 0.45. Both figures show a delay in $C_{p_{min}}$ development about 1.5 deg for k = 0.1 when compared to the steady flow case. But, the peak suction attained by the untripped airfoil in the two unsteady cases is the same at -4.3, and is higher than the value of about -3.8 when the flow is steady. These are higher than the critical value and hence, the flow becomes supersonic in all cases. Fig. 17b shows $C_{p_{min}}$ to be increasing for k = 0.1 even at $\alpha = 12^0$ in the tripped case. The PDI pictures show (see Fig. 9) that the dynamic stall process is already under way at this condition from a shock-induced flow separation at a downstream x/c location of about 0.05. It appears that the locally supersonic flow upstream is not affected until the separation location moves upstream to the leading edge for such cases.

4.B.2.6. Comparison of Global Pressure Distribution at M = 0.45

Figure 18 compares the global pressure distributions for the 3-inch and the 6-inch airfoils. Fig. 18a and 18b are pressure maps pertaining to the 3-inch untripped and tripped cases respectively. Fig. 18c and 18d are for the corresponding 6-inch cases. Of interest is the extent of the supersonic region surrounded by the sonic line, $C_p = -2.76$. All cases show multiple shocks. However, the supersonic region extends to x/c = 0.12 in

Fig. 18a whereas in Fig. 18b it has a long tail extending to x/c = 0.15. The shape of the region is also different in these two cases. The untripped 6-inch airfoil flow shows that the supersonic region extends to about x/c = 0.06, Fig. 18c, terminating in a shock. At the foot of the shock, the flow separates as described in Sec. 4.B.1.2. producing a dynamic stall vortex. Fig. 18d shows the smallest supersonic region, extending from the suction peak to x/c = 0.045, which also terminates in a shock that induces flow separation causing dynamic stall. There are some differences in the outer regions of the flow, but the most significant are within the supersonic region of the flow. The region shrinks with increasing Reynolds numbers as Fig. 18 demonstrates. A logical extension of this result will lead to the conclusion that, at much higher Reynolds numbers, the supersonic region becomes even smaller and eventually terminates in a strong shock from which dynamic stall arises.

4.B.3. Inclusion of Transition Modeling in Computations

The flow over an untripped airfoil at the low Reynolds numbers of model-scale experiments, such as the present one, is substantially influenced by the formation of a laminar separation bubble. For the bubble to close, the separated laminar shear layer has to undergo transition. The details of the transition process are affected by the flow conditions and airfoil oscillation parameters. The transition onset point and length vary dramatically over the airfoil as it pitches-up and develops an increasingly strong adverse pressure gradient. It is naturally a complex process occurring near the airfoil leading edge where compressible dynamic stall also originates, this creates a strong dependence of the flow on transition. Most computational studies have not included a proper transition model. This was attempted in the doctoral dissertation of Ref. 14. In this study, the transition onset point was systematically varied from the initial prediction given by Michel's criterion, which is based on high Reynolds number data, $Re \geq 10^6$. The transition length was varied by changing a constant in the well known Chen-Thyson transition model. The model uses a turbulent intermittency distribution γ_{tr}, developed from data for attached flows and gives the turbulent intermittency as:

$$\gamma_{tr}(x) = 1 - exp\Big[\Big(-\frac{u_e^3}{G_{\gamma_{tr}}\nu^2}\Big)Re_{x_{tr}}^{-1.34}(x - x_{tr})\int_{x_{tr}}^{x}\frac{dx}{u_e}\Big]$$

At the low Reynolds number of the present experiments, it was necessary (Walker et al, Ref. 15) to reduce the value of the transition constant $G_{\gamma_{tr}}$ ($50 \leq G_{\gamma_{tr}} \leq 450$) to properly compute the separation bubble, from the recommended value of 1200 for high Reynolds number flows. Physically, a lower value of the transition constant forces transition to complete over a shorter distance as is the case prior to onset of dynamic stall. The transition length was varied from an initial estimate given by the Cebeci correlation formula

$$G_{\gamma_{tr}} = 213[log(Re_{x_{tr}}) - 4.7323]/3.$$

The value that best models the separation bubble behavior observed in the experiments for the angle of attack variation $\alpha = 10^0 - 2^0 \sin \omega t$ was used to compare the results. The extreme sensitivity of the flow to these parameters made it critical to make the choices very carefully. Subsequently, the Baldwin-Barth one equation model was used for computation of the eddy viscosity in the fully turbulent region.

Satisfactory agreement with experimental data was obtained in steady flow and for the upstroke of the airfoil at M = 0.3 and k = 0.05. Results for the downstroke were affected by the abrupt shedding of the vorticity that caused light dynamic stall. Ref. 14 provides more complete details of the procedure followed and the results for various conditions.

4.B.4. Results of Preliminary Tests of the DDLE Airfoil

Figure 19 represents some of the shapes that were tested. Shape 0 is nearly identical to the 6-inch chord NACA 0012 airfoil. Each shape increment corresponds to a retraction of the leading edge by 0.003 in. The rapid reduction of the leading edge curvature is clear from it even for such small movements.

4.B.4.1. Flow Over Different Shapes

Flow interferograms over shapes 0, 9, 13 and 17 are shown for M = 0.3 and $\alpha = 18$ deg. In this case, the airfoil was held at 18 deg and with the flow on, the nose was retracted to these different shapes and maintained there until the images were acquired. The basic NACA 0012 airfoil stalled at 14 deg as did the shape 0 airfoil. Hence, fully separated flow is seen from the leading edge for this case in Fig. 20a. For shape 9, Fig. 20b, the

flow appears fully reattached as all the fringes gradually turn over the leading edge and follow the boundary layer. The presence of a large number of fringes near the leading edge indicates that the airfoil is producing suction again, confirming that the fully stalled flow has reattached. For shape 13, a laminar separation bubble can be seen in Fig. 20c, which also appears to be breaking down. For this case, the fringes slightly downstream of the bubble are lifting off the surface, pointing to the possibility of trailing edge stall propagating upstream. Also, there are fewer leading edge fringes than seen for shape 9. Eventually, the flow separates when shape 17 is formed. These images demonstrate the success of the DDLE airfoil in achieving flow separation control by favorably modifying the flow gradients as the airfoil shape is changed. By studying a large number of images at different angles of attack and over different shapes, Fig. 21 has been drawn to determine the conditions over which the DDLE works satisfactorily. In Fig. 21a for M = 0.3, a scan along a horizontal axis shows that there exists a window of shapes in which initially separated flow can be *made to reattach fully.* Outside of this window, the airfoil flow seems partially attached for some conditions before it experiences leading edge stall. A similar result was obtained for M = 0.45, Fig. 21b. But, the window size decreases considerably with increasing Mach number (Ref. 16). It is important to note that for this higher Mach number case, there are multiple shocks present in the flow and these can induce local separation while the leading edge flow is attached producing a large suction there.

4.B.4.2. Distribution of Vorticity Flux Over the DDLE Airfoil

Using the pressure distributions derived from the PDI images, the vorticity flux over the airfoil was calculated by fitting a cubic spline to the distributions from the expression (Ref. 17)

$$\nu \frac{\partial \Omega}{\partial n} = \frac{1}{\rho} \frac{\partial p}{\partial s}$$

Typical distributions are shown in Fig. 22 for three angles of attack at M = 0.3. The peak value in Fig. 22a for $\alpha = 12$ deg occurs for the shape 0 airfoil near the leading edge, whereas for the other shapes, the distributions show nearly zero value here, and flatter positive values further downstream. In Fig. 22b, for $\alpha = 14$ deg, the peak value for shape

0 has begun to drop (as stall becomes imminent), where as for shapes 8 and 10, the peak vorticity flux has increased substantially over that seen in Fig. 22a. Also, a peak has formed near the leading edge for shapes 4 and 8. At $\alpha = 18$ deg, the peak has begun to fall as stall sets in for these shapes. The favorable redistribution of the vorticity flux in this figure for selected shapes and the delay of flow separation have been brought about by changes to the airfoil shape. This validates the DDLE airfoil concept for flow control.

4.B.4.3. Flow Past Oscillating Shape 8 Airfoil

In examining Fig. 21a, it can be seen that the flow over shape 8 airfoil is fully attached up to $\alpha = 18$ deg. In view of this, this particular shape was tested with the airfoil oscillating. The data was obtained using the high-speed Cordin camera by recording 200 images in the cycle by imaging at the rate of 10 KHz. By changing the angle of attack where the imaging sequence was initiated, the flow over the airfoil for the entire cycle was recorded. These images showed **NO** dynamic stall vortex over any portion of the cycle! Fig. 23 presents representative interferograms for this case. All these show the leading edge flow to be attached. Occasional trailing edge flow separation can be seen, but the dynamic stall vortex is conspicuous by its absence. This extraordinary flow situation will be studied further in the near future.

4.B.5. Conclusions

A study of the compressible dynamic stall flow over fixed and adaptive geometries has been carried out. Stroboscopic point diffraction interferometry was used to obtain single exposure images as well as 200 high-speed images of the flow. Reynolds number effects were documented by using two different airfoils but testing them at the **same** Mach number. Additionally, tripping the airfoils enabled achieving a higher "equivalent" Reynolds number for each airfoil.

The study revealed for the first time that there are at least three mechanisms that can cause compressible dynamic stall. These are:

1. bursting of a laminar separation bubble
2. shock-induced flow separation

3. a complex interaction between the local supersonic flow and the bubble that results in a competition amongst the above mechanisms of dynamic stall depending upon *small* changes in the flow conditions in the transonic regime.

Based on how the dynamic stall process was initiated, the imprint of the vortex in the flow changes from nearly circular in the first case to an oval shape in the second case due to the external boundary condition imposed on its development. These results are strongly affected by both Reynolds number and Mach number, with compressibility effects dominating at higher Reynolds numbers. This implies that care is required before applying model-scale results to full-scale conditions since the physical processes involved are significantly different.

Increasing Reynolds number progressively increases the airfoil peak suction pressure at a given angle of attack. The supersonic flow that forms at the higher Reynolds number can produce a strong shock that induces dynamic stall. By comparing with full-scale Reynolds number data, it was established that by tripping a 6-inch NACA 0012 airfoil at M = 0.3 the full-scale Reynolds number effects can be reasonably simulated. The same result was not obtained for the 3-inch airfoil indicating that a minimum untripped Reynolds number of 1×10^6 may be needed for a successful simulation.

It was found that satisfactory agreement of the computational results with experiments can be obtained by better modeling of transition to include the variation of the transition onset location and transition length as the airfoil pitches-up.

DDLE airfoil tests showed that fully separated flow can be effectively reattached by changing the airfoil shape suitably. As much as **six** degrees of **stall delay** was achieved at M = 0.3 in steady flow by this approach. A re-distribution of the vorticity flux was found to be responsible for this result. A special airfoil shape was found which does **NOT** produce a dynamic stall vortex at M = 0.3, k = 0.05.

4.C. LIST OF PUBLICATIONS AND TECHNICAL REPORTS

1. L.W.Carr, and M.S.Chandrasekhara, "Compressibility Effects on Dynamic Stall", **Invited Paper** *Progress in Aerospace Sciences*, Vol. 32, pp. 523-576, 1996.

2. R.D.Van Dyken, J.A.Ekaterinaris, M.S.Chandrasekhara, and M.F.Platzer, "Analysis of Compressible Light Dynamic Stall Flow at Transitional Reynolds Numbers", (AIAA Paper No. 94-2255), *AIAA Journal*, Vol. 34, No. 7, Jul. 1996, pp. 1420-1427.

3. M.S.Chandrasekhara, M.C.Wilder, and L.W.Carr, "Boundary Layer Tripping Studies of Compressible Dynamic Stall Flow", (AIAA Paper No. 94-2340), *AIAA Journal*, Vol. 34, No. 1, Jan. 1996, pp. 96-103.

4. M.S.Chandrasekhara, D.D.Squires, M.C.Wilder, and L.W.Carr, "A Phase-Locked High-Speed Real-Time Interferometry System for Large Amplitude Unsteady Flows", *Experiments in Fluids*, Vol. 20, Dec. 1995, pp. 61-67.

5. M.C.Wilder, M.S.Chandrasekhara, L.W.Carr, "Computer-Aided Analysis of Interferometric Images of Unsteady Aerodynamic Flows", ICIASF'95 RECORD, *IEEE Publication 95-CH3482-7*, pp. 44.1 - 44.11.

6. M.S.Chandrasekhara, and L.W.Carr, "Compressibility Effects on Dynamic Stall of Oscillating Airfoils", *AGARD-CP-552*, Oct. 1994, pp. 3.1 - 3.15.

7. J.A.Ekaterinaris, M.S.Chandrasekhara, and M.F.Platzer, "Analysis of Low Reynolds Number of Airfoil Flows", (AIAA Paper 94-0534), *Journal of Aircraft*, Vol. 32, No. 3, May-Jun. 1995, pp. 625-630.

8. M.S.Chandrasekhara, M.C.Wilder and L.W.Carr, "Control of Flow Separation Using Adaptive Airfoils", *AIAA Paper 97-0655*, Reno, NV, Jan. 1997.

9. M.F.Platzer and M.S.Chandrasekhara, "Research on Dynamic Stall Onset and Stall Flutter", *Workshop on Active Blade Vibration Control*, Wright Patterson Air Force Base, OH, Aug. 14-15, 1996.

10. M.S.Chandrasekhara, M.C.Wilder, and L.W.Carr, "On the Competing Mechanisms

of Compressible Dynamic Stall", *AIAA Paper 96-1953*, New Orleans, LA, Jun. 1996, *To Appear in AIAA Journal.*

11. M.S.Chandrasekhara, M.C.Wilder, and L.W.Carr, "Reynolds Number Influence on 2-D Compressible Dynamic Stall", *AIAA Paper 96-0073*, Reno, NV, Jan. 1996

12. L.W.Carr, M.S.Chandrasekhara, and S.S.Davis, "Flow Control for Unsteady Separated Flow", *Proc. NASA Langley Workshop on Enabling Technologies for Smart Aircraft Systems*, Hampton, VA, May 1996.

13. M.S.Chandrasekhara, L.W.Carr, and M.C.Wilder, "Unsteady Aspects of Compressible Dynamic Stall Flow at Very Low Pitch Rates", *Proc. 6^{th} Asian Congress of Fluid Mechanics*, Singapore, May. 22-26, 1995, Vol. II, pp. 1528-1531.

14. L.W.Carr and M.S.Chandrasekhara, "A Review of Compressibility Effects on Dynamic Stall of Airfoils", *AIAA Paper 95-0779*, **Invited Paper**, Reno, NV, Jan. 1995.

Thesis Completed:

1. R.D.Van Dyken, "Experimental and Computational Analysis of Separation Bubbles for Compressible Steady and Oscillatory Flows Over a NACA 0012 Airfoil at $M_\infty = 0.3$ and Re = 540,000", Ph. D. Thesis, Department of Aeronautics and Astronautics, Naval Postgraduate School, Monterey, CA, Mar. 1997.

4.D. LIST OF ALL PARTICIPATING PERSONNEL

1. Professor M.S.Chandrasekhara, NPS, Monterey, CA
2. Professor M.F.Platzer, NPS, Monterey, CA
3. Mr. R.D.Van Dyken, Ph.D. Student, NPS, Monterey, CA
4. Dr. L.W.Carr, Cooperative participant, Group Leader, U.S. Army AvRDEC & ATCOM, Moffett Field, CA
5. Dr. M.C.Wilder, Senior Research Scientist, MCAT Inc..

5. REPORT OF INVENTIONS

None.

6. BIBLIOGRAPHY

1. Chandrasekhara, M.S., Wilder, M.C., and Carr, L.W., "Boundary Layer Tripping Studies of Compressible Dynamic Stall Flow", (AIAA Paper No. 94-2340), *AIAA Journal*, Vol. 34, No. 1, Jan. 1996, pp. 96-103.

2. Chandrasekhara, M.S., Carr, L.W., and Wilder, M.C., "Development of High Speed Imaging and Analysis Techniques for Compressible Dynamic Stall", To be presented at the *AGARD* 81^{st} *Meeting and Symposium on Advanced Aerodynamic Measurement Technology*, Seattle, WA, Sep. 22-25, 1997.

3. Chandrasekhara, M.S., Carr, L.W., Wilder, M.C., Paulson, G.N., and Sticht, C.D., "Design and Development of a Dynamically Deforming Leading Edge Airfoil for Unsteady Flow Control", To be presented at the 17^{th} *International Conference on Instrumentation in Aerospace Simulation Facilities*, Monterey, CA, Sep. 29 - Oct. 2, 1997.

4. Wilder, M.C., Chandrasekhara, M.S., Carr, L.W., "Computer-Aided Analysis of Interferometric Images of Unsteady Aerodynamic Flows", ICIASF'95 RECORD, *IEEE Publication 95-CH3482-7*, pp. 44.1 - 44.11.

5. Chandrasekhara, M.S., and Carr, L.W., "Compressibility Effects on Dynamic Stall of Oscillating Airfoils", *AGARD-CP-552*, Oct. 1994, pp. 3.1 - 3.15.

6. Cho, Y.C., Carr, L.W., and Chandrasekhara, M.S., "Corrections to Fringe Distortion due to Flow Density Gradients in Optical Interferometry", *AIAA Paper 93-0631*, Reno, NV, Jan. 1993.

7. Chandrasekhara, M.S., Wilder, M.C., and Carr, L.W., "Reynolds Number Influence on 2-D Compressible Dynamic Stall", *AIAA Paper 96-0073*, Reno, NV, Jan. 1996

8. Carr, L.W., Chandrasekhara, M.S., and Brock, N.J., "A Quantitative Study of Unsteady Compressible Flow on an Oscillating Airfoil", (AIAA Paper 91-1683), *Journal of Aircraft*, Vol. 31, No. 4, Jul.- Aug. 1994, pp.892 - 898.

9. Chandrasekhara, M.S., Wilder, M.C., and Carr, L.W., "On the Competing Mecha-

nisms of Compressible Dynamic Stall", *AIAA Paper 96-1953*, New Orleans, LA, Jun. 1996, *To Appear in AIAA Journal.*

10. Guderley, G., "On the Presence of Shocks in Mixed Subsonic-Supersonic Flow Patterns", *Advances in Applied Mechanics*, Vol. III, Academic Press Inc., New York, 1953, pp. 145-184.

11. Conger, R.N. and Ramaprian, B.R., "Pressure Measurements on a Pitching Airfoil in a Water Channel", *Report No. MME-TF-92-3*, Wash. St. Un., Dept. of Mech. and Materials Engg., Pullman, WA, May 1992.

12. Lorber, P.F. and Carta, F.O., "Unsteady Stall Penetration Experiments at High Reynolds Number", *Report NO. AFOSR TR-87-1202 & UTRC R87-956939-3*, United Tech. Res. Center, East Hartford, CT, Apr. 1987

13. McAlister, K.W., Pucci, S.L., McCrokey, W.J., and Carr, L.W., "An Experimental Study of Dynamic Stall on Advanced Airfoil Sections, Vol. 2: Pressure and Force Data", NASA TM-84245, USAAVRADCOM TR-82-A-8, Sep. 1982.

14. Van Dyken, R.D., "Experimental and Computational Analysis of Separation Bubbles for Compressible Steady and Oscillatory Flows Over a NACA 0012 Airfoil at $M_\infty = 0.3$ and Re = 540,000", Ph. D. Thesis, Department of Aeronautics and Astronautics, Naval Postgraduate School, Monterey, CA, Mar. 1997.

15. Walker, G.J., Subroto, P.H., and Platzer, M.F., "Transition Modeling Effects on Viscous/Inviscid Interaction Analysis of Low Reynolds Number Airfoil Flows Involving Laminar Separation Bubbles", *ASME Paper 92-GT380.* Jun. 1992.

16. Chandrasekhara, M.S., Wilder, M.C. and Carr, L.W., "Control of Flow Separation Using Adaptive Airfoils", *AIAA Paper 97-0655*, Reno, NV, Jan. 1997.

17. Reynolds, W.C., and Carr, L.W., "Review of Unsteady, Driven, Separated Flows", *AIAA Paper 85-0527*, Mar. 1985.

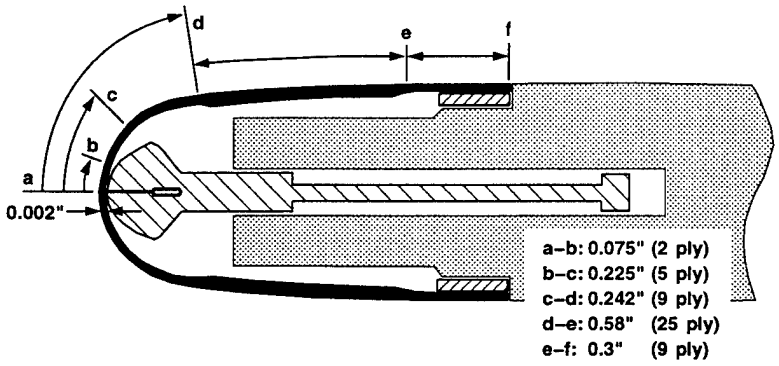

Fig. 1. Construction Details of the DDLE Airfoil Model.

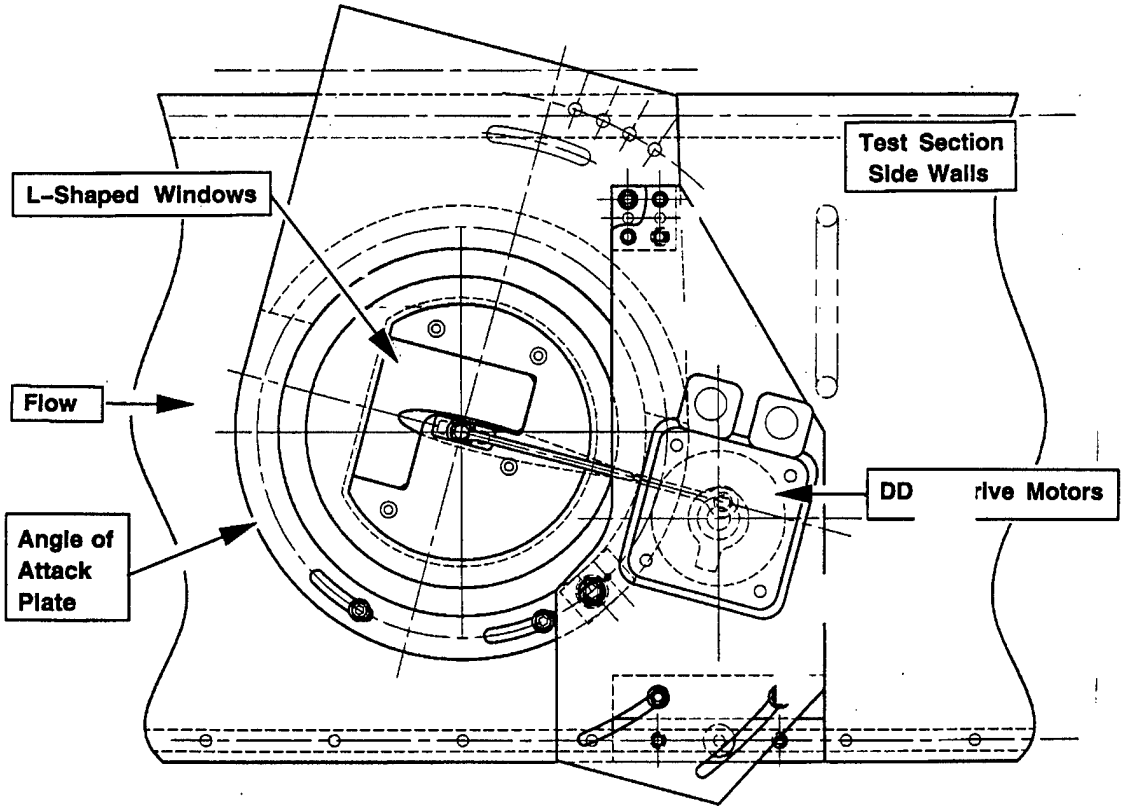

Fig. 2. Schematic of the DDLE Drive System on the CDSF.

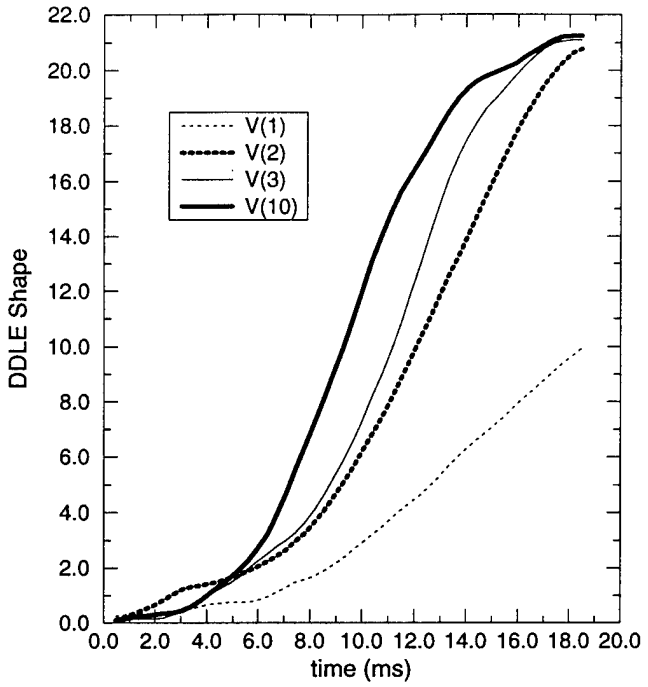

Fig. 3. DDLE Motion History for Different Rates, V.

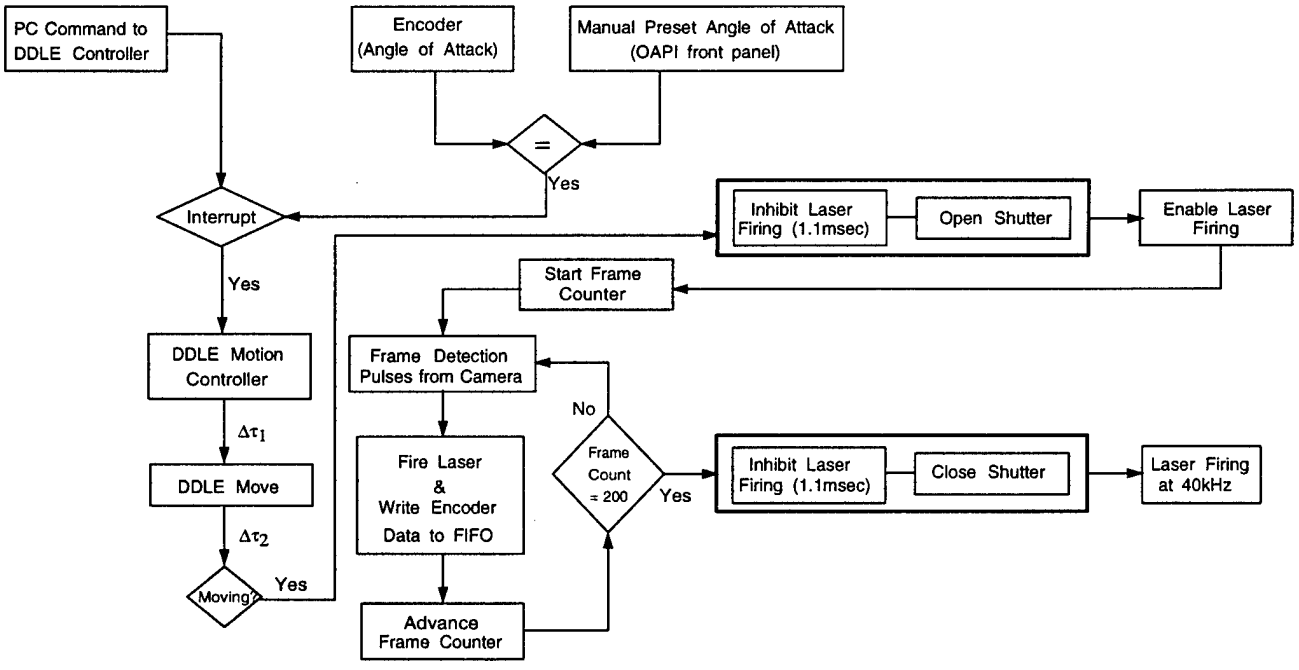

Fig. 4. Phase Interlocking of DDLE, CDSF, Pulsed Laser and High-Speed Camera.

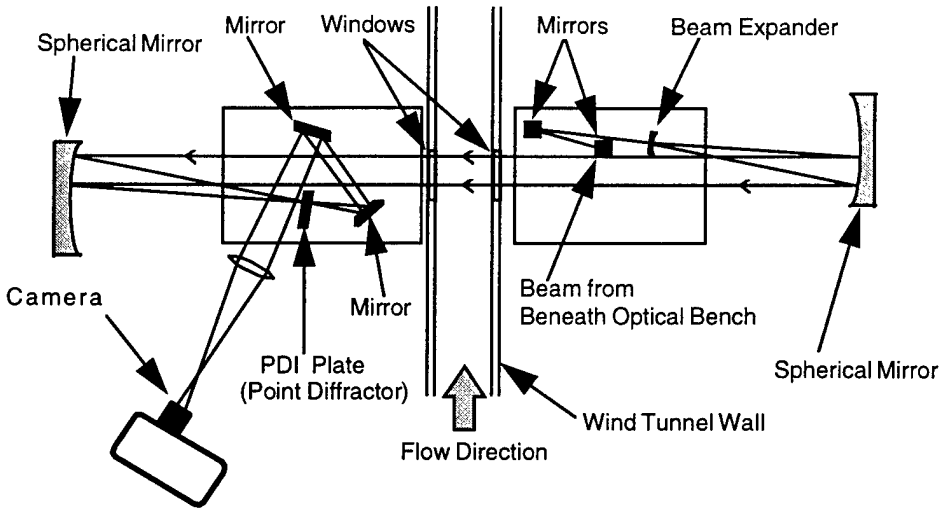

Fig. 5. Schematic of the Point Diffraction Interferometry System.

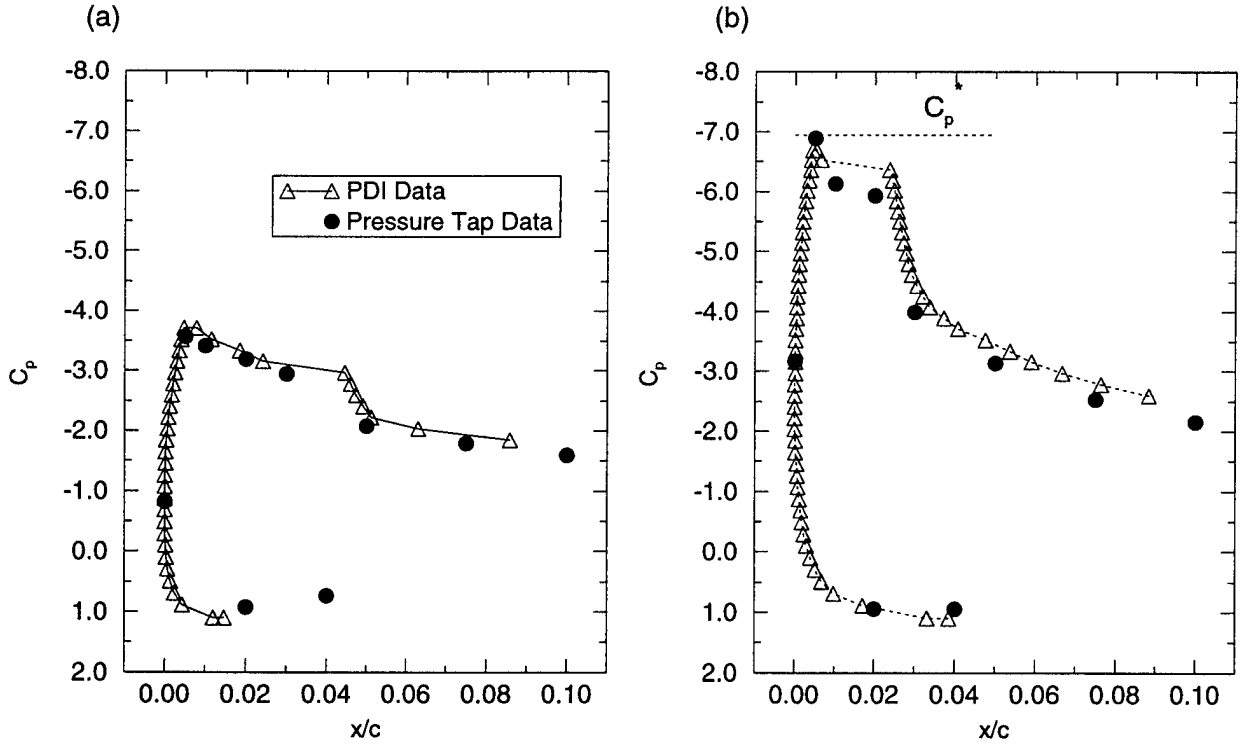

Fig. 6. Comparison of Pressure Tap Measurements with PDI Derived Pressure Coefficient Distribution; M = 0.3, k = 0. (a) $\alpha = 8.0^0$, (b) $\alpha = 13.0^0$.

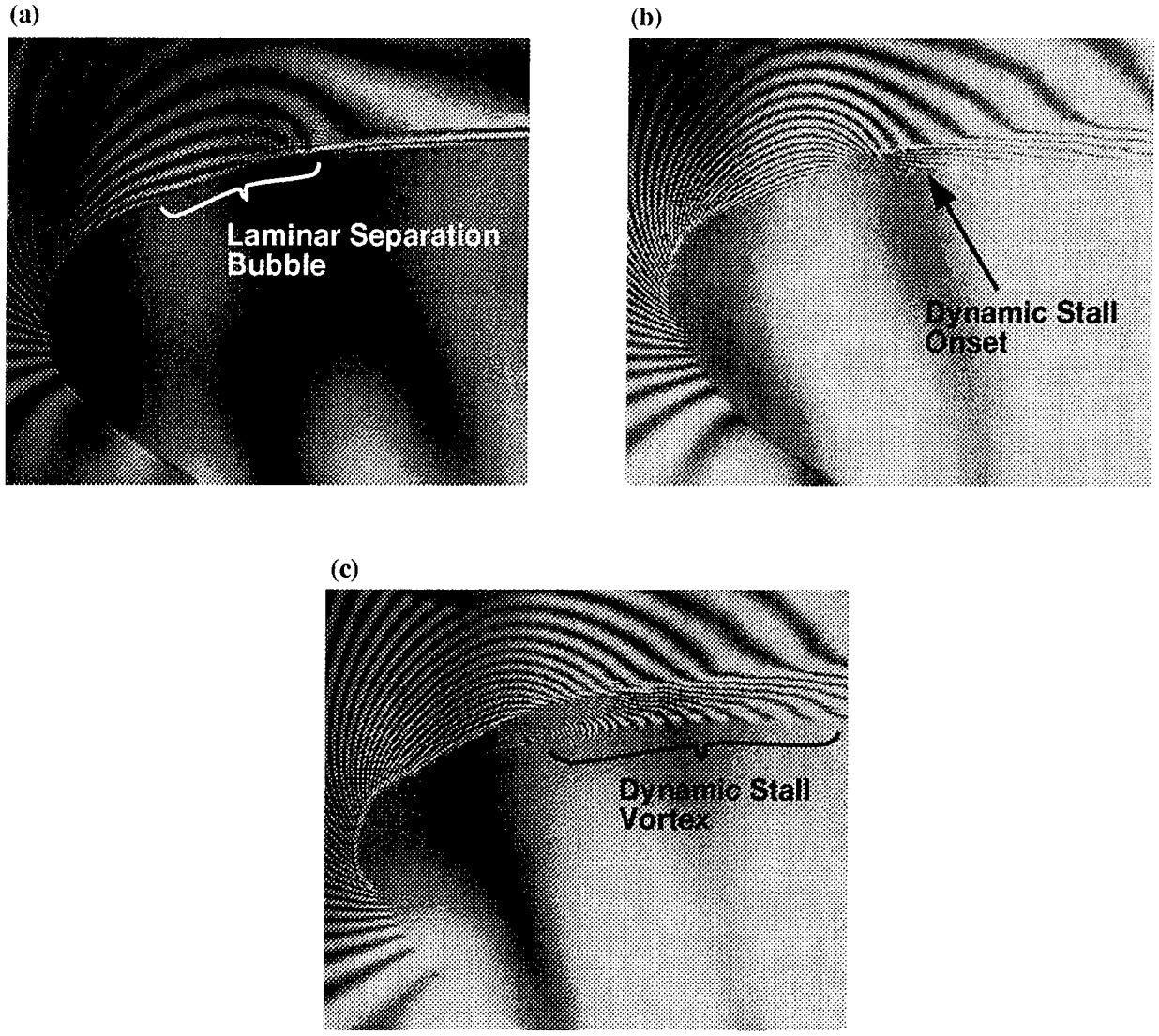

Fig. 7. PDI Images Illustrating Laminar Separation Bubble Induced Dynamic Stall, M = 0.3, k = 0.05, Untripped 6–inch Airfoil. (a) $\alpha = 8.98^{\circ}$, (b) $\alpha = 12.47^{\circ}$, (c) $\alpha = 13.48^{\circ}$.

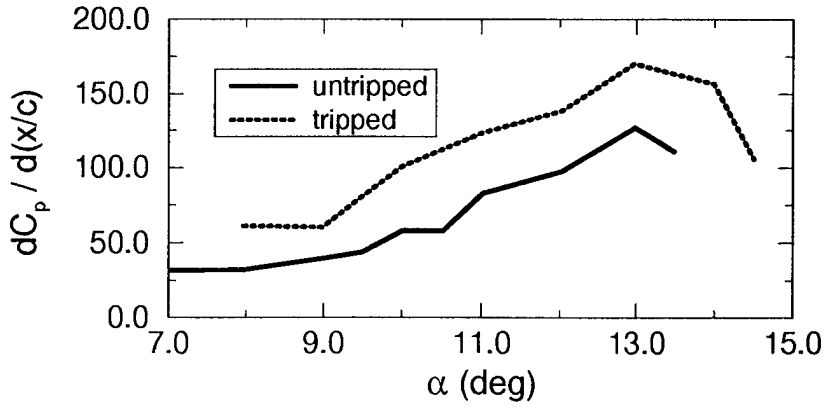

Fig. 8. Adverse Pressure Gradient Development for the 6–inch Airfoil, M = 0.3, k = 0.05, $\alpha = 10^{\circ} - 10^{\circ} \sin\omega t$.

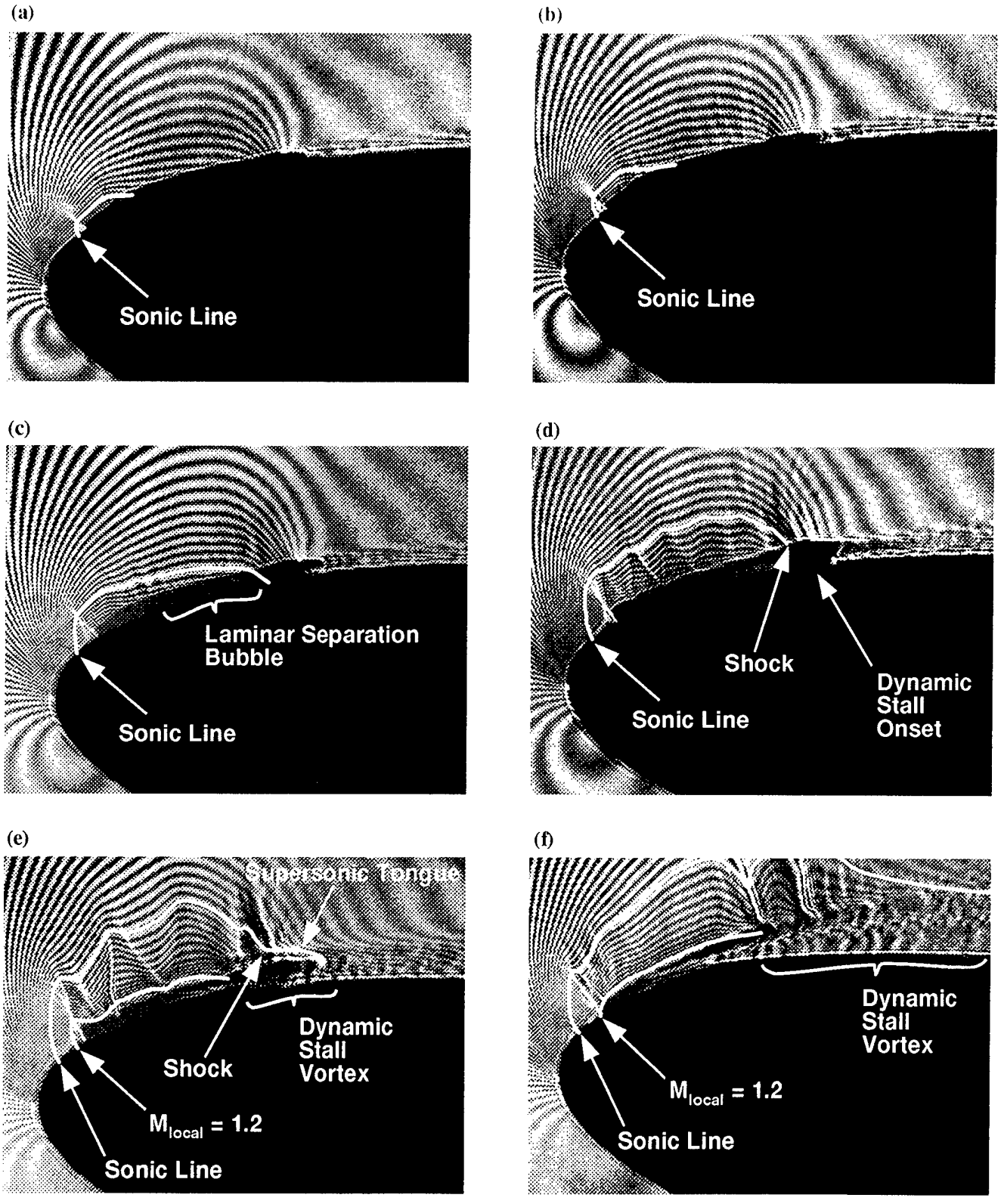

Fig. 9. PDI Images Illustrating Shock Induced Dynamic Stall, M = 0.45, k = 0.05, Untripped 6–inch Airfoil. (a) α =7.53°, (b) α =7.97°, (c) α = 8.40°, (d) α = 8.98°, (e) α = 9.49°, (f) α = 10.72°.

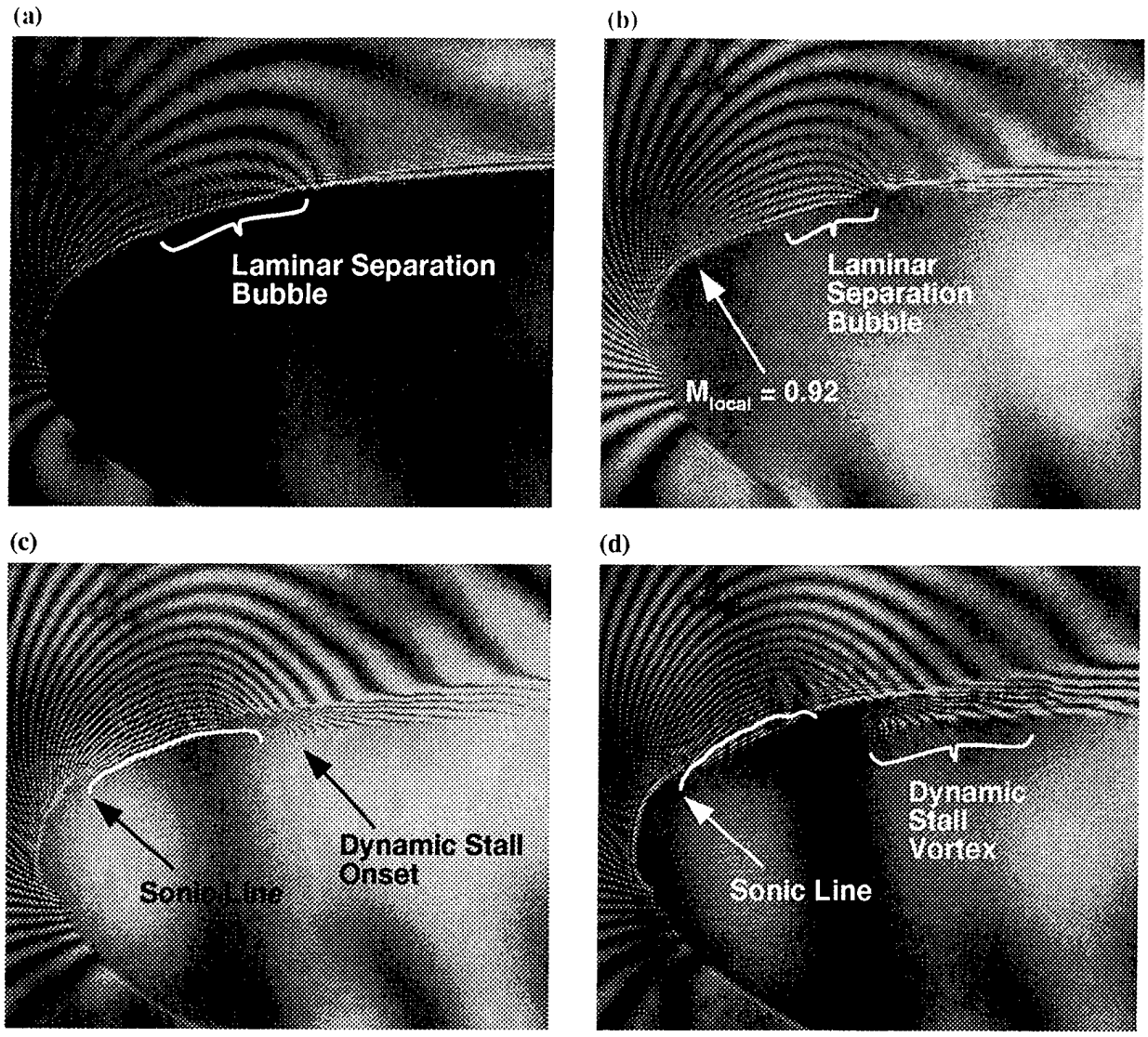

Fig. 10. PDI Images Illustrating Dynamic Stall Onset from Interactions of Laminar Separation Bubble and Supersonic Flow, M = 0.35, k = 0.05, Untripped 6–inch Airfoil.
(a) $\alpha = 7.97^{\circ}$, (b) $\alpha = 10.00^{\circ}$, (c) $\alpha = 11.52^{\circ}$, (d) $\alpha = 12.03^{\circ}$.

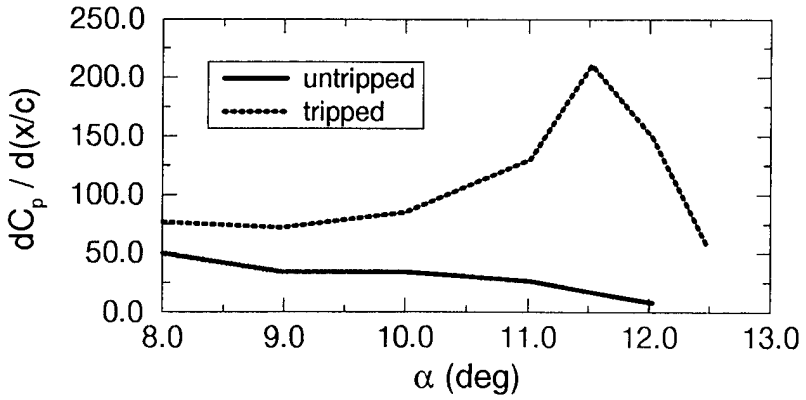

Fig. 11. Adverse Pressure Gradient Development for the 6–inch Airfoil, M = 0.35, k = 0.05.

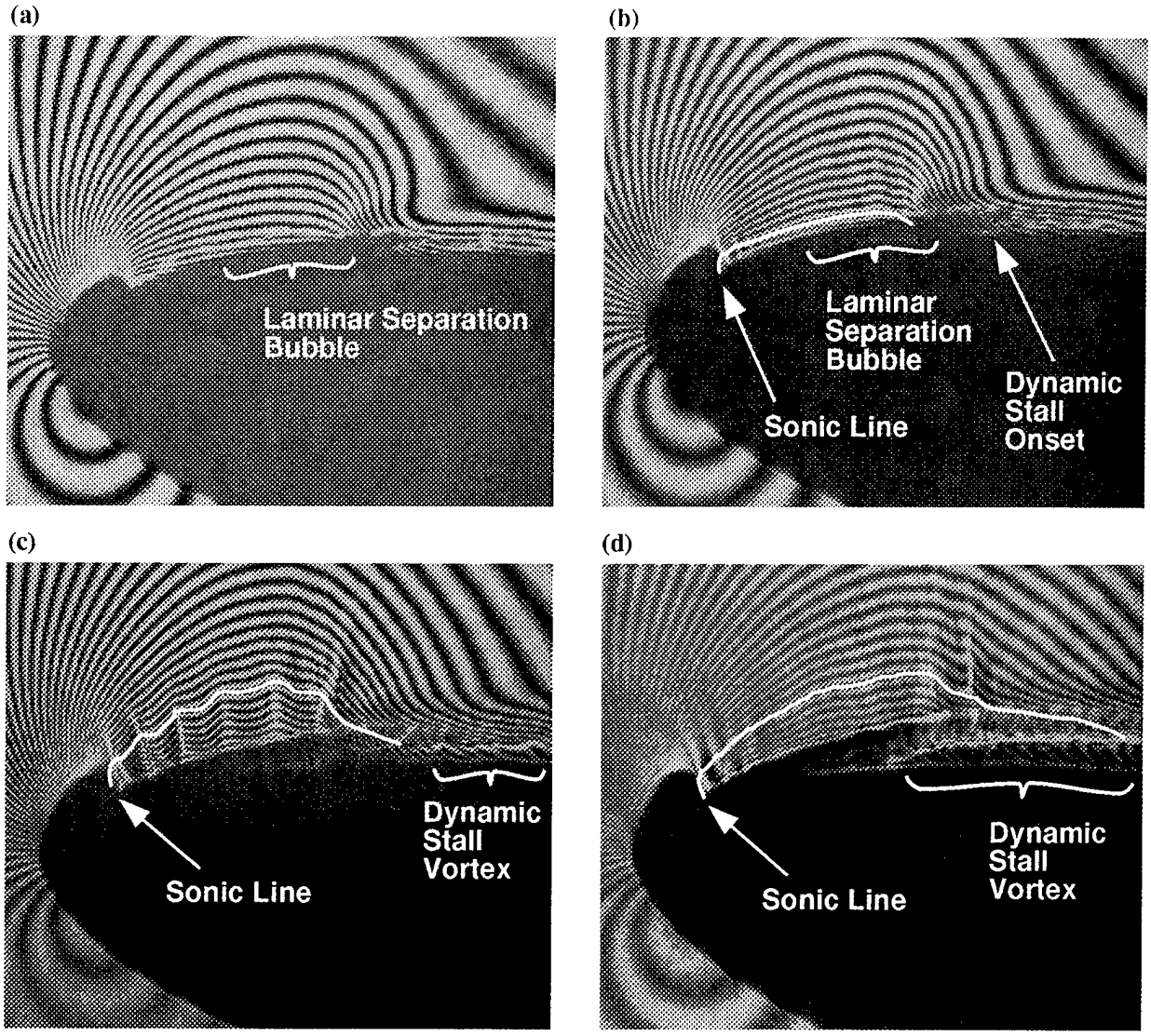

Fig. 12. PDI Images Illustrating Dynamic Stall Onset from Interactions of Laminar Separation Bubble and Supersonic Flow, M = 0.45, k = 0.05, Untripped 3-inch Airfoil.
(a) $\alpha = 8.48^{o}$, (b) $\alpha = 8.98^{o}$, (c) $\alpha = 10.00^{o}$, (d) $\alpha = 11.02^{o}$.

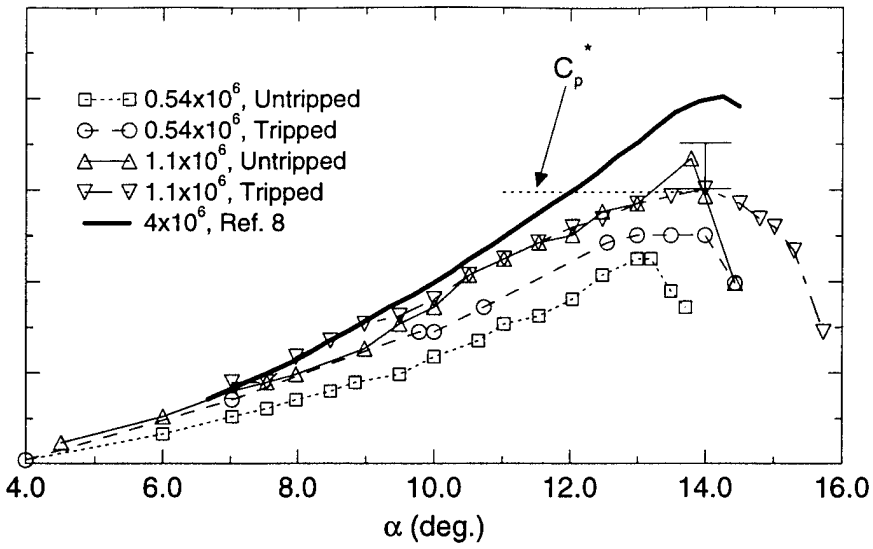

Fig. 13. Reynolds Number Effect on Airfoil Suction Peak Development, M = 0.3, k = 0.

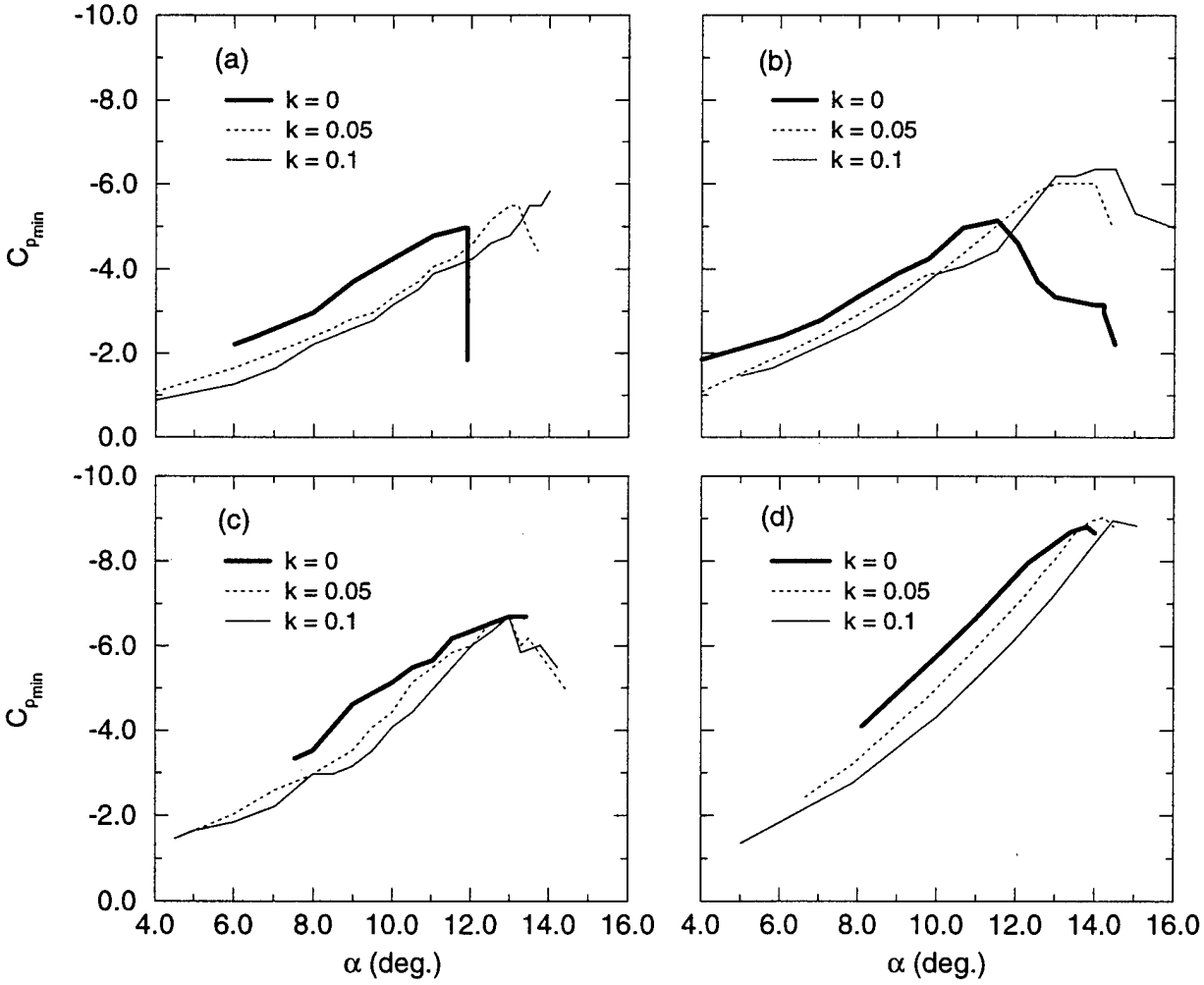

Fig. 14 Effect of Unsteadiness on Airfoil Suction Peak Development, M = 0.3. (a) Re = 0.54×10^6, (b) Re = 0.54×10^6, Tripped, (c) Re = 1.1×10^6, (d) Re = 4×10^6.

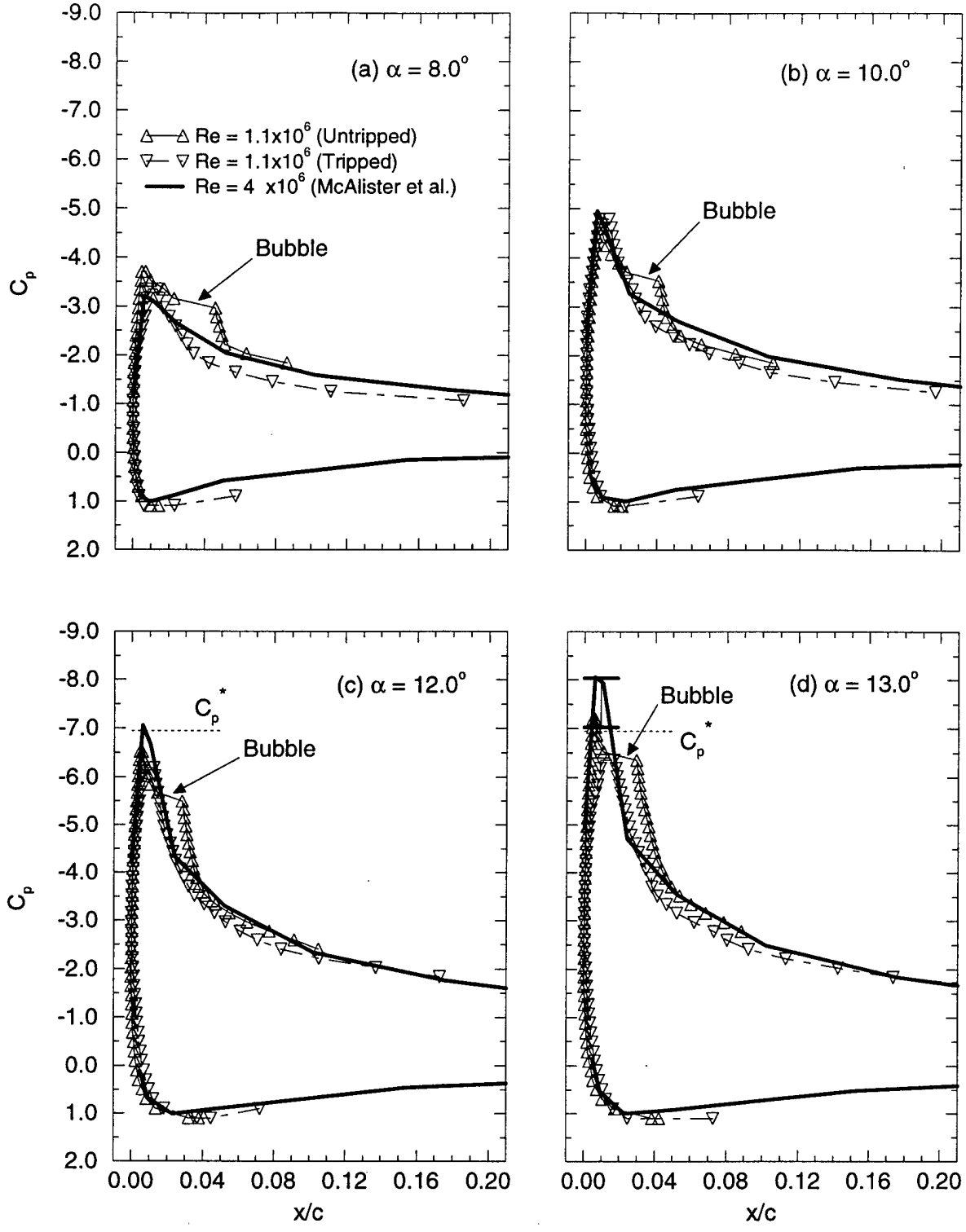

Fig. 15 Effect of Reynolds Number on Airfoil Pressure Distribution, M = 0.3, k = 0.05.

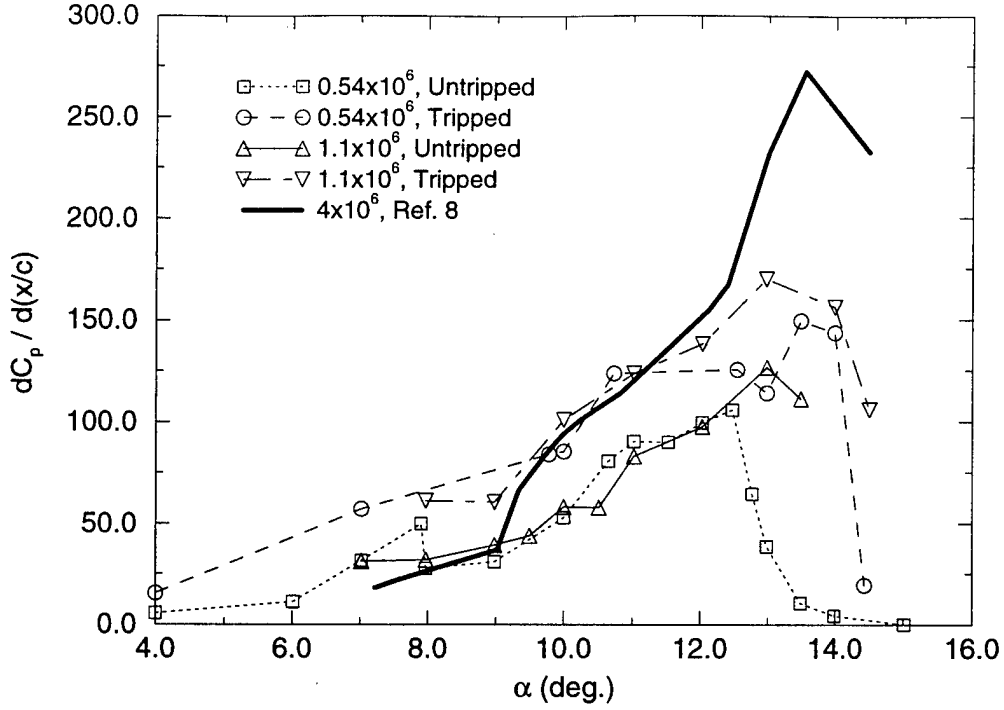

Fig. 16. Reynolds Number Effect on Adverse Pressure Gradient Development, M = 0.3, k = 0.05.

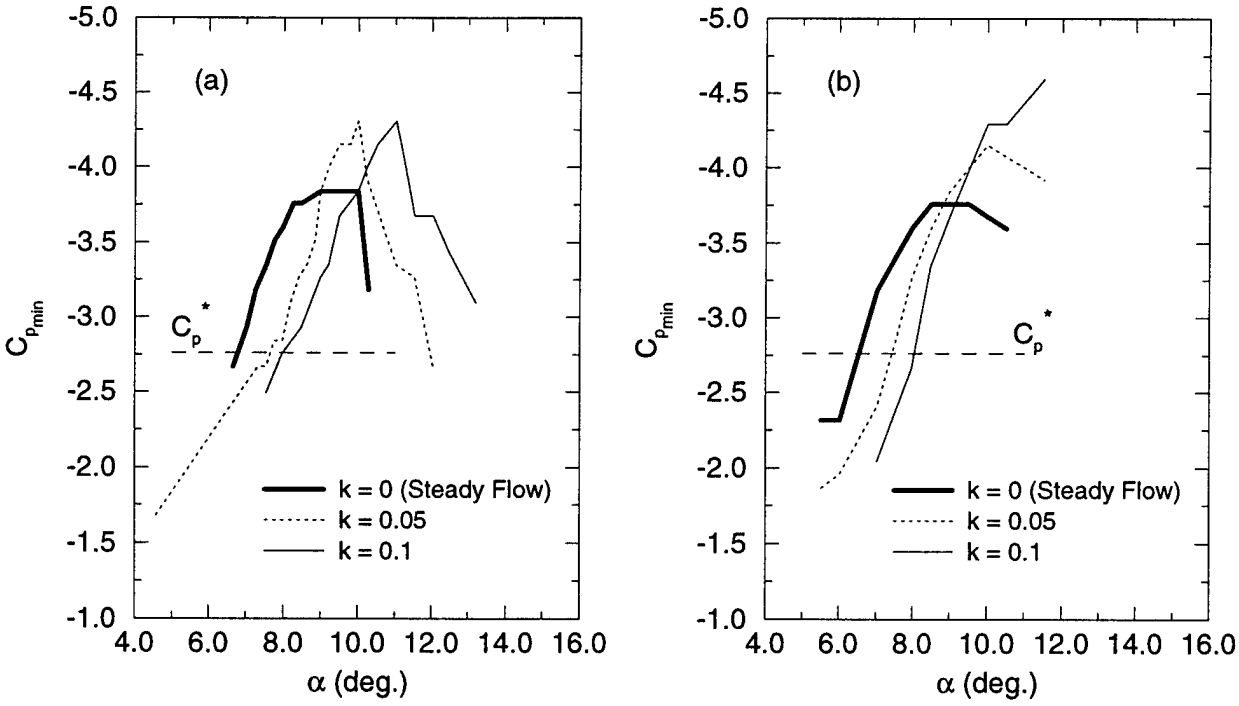

Fig. 17. Effect of Unsteadiness on Airfoil Suction Peak Development, M = 0.45, Re = 1.6x10^6. (a) Untripped, (b) Tripped.

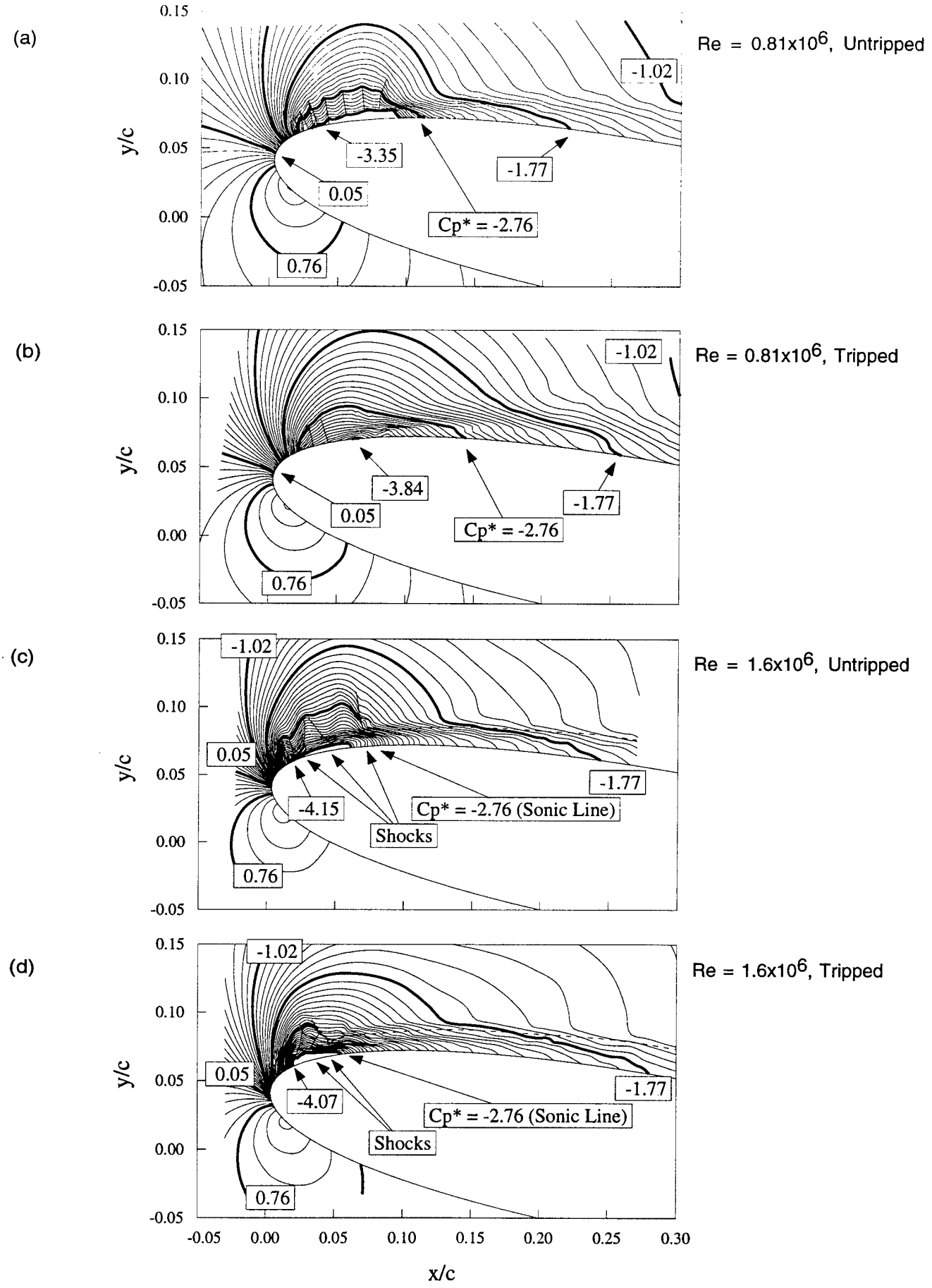

Fig. 18. Global Pressure Coefficient Distributions, M = 0.45, k = 0.05, $\alpha = 10^{o}$.

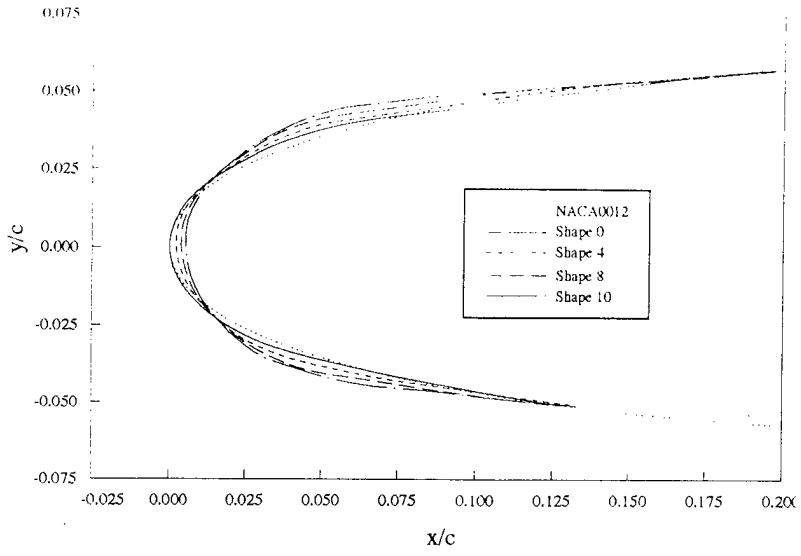

Fig. 19. DDLE Shape Profiles Compared with the NACA 0012 Profile.

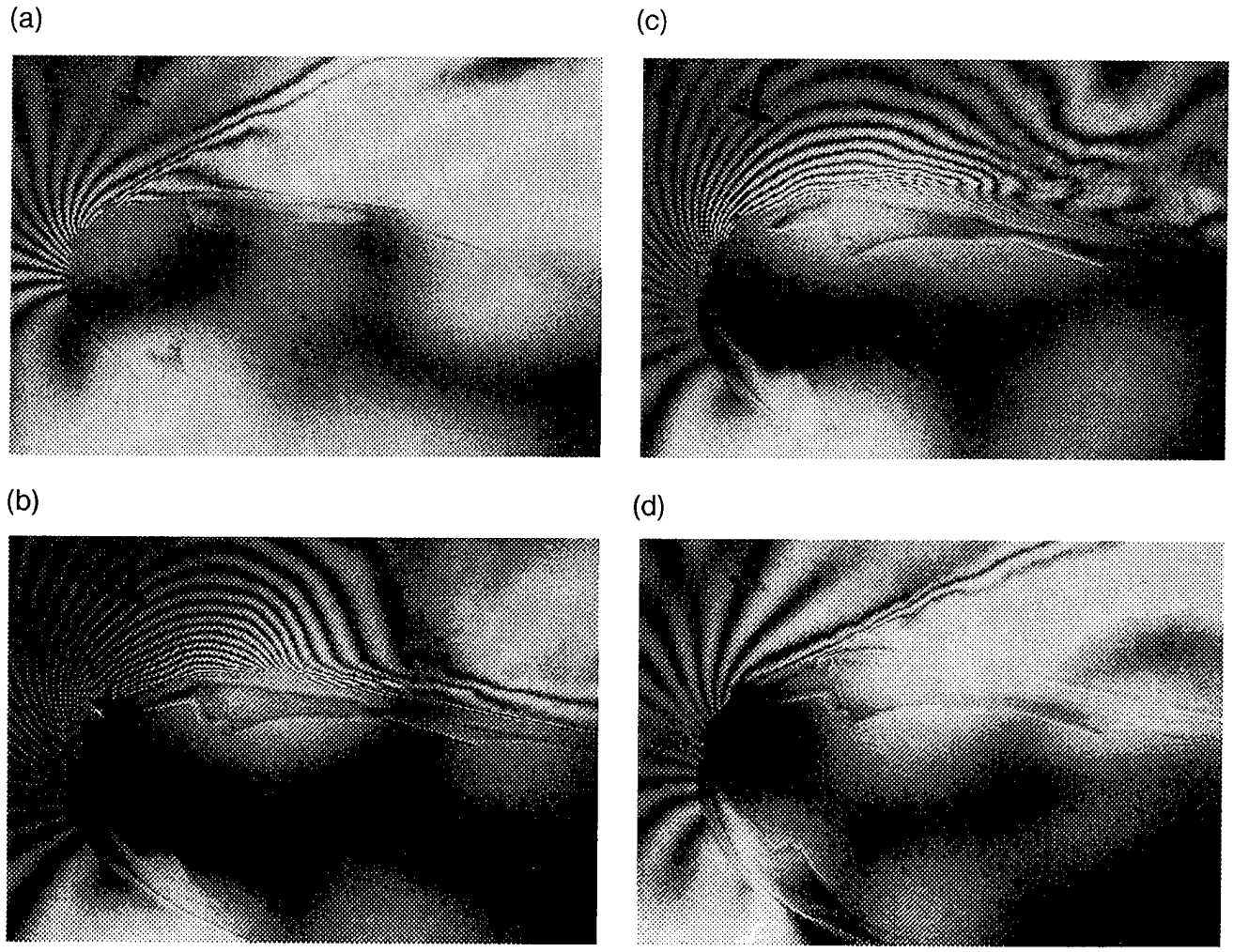

Fig. 20. Flow Modification with Changing Leading Edge Shape, M = 0.3, k = 0, α = 18.00°
(a) Shape 0, (b) Shape 9, (c) Shape 13, (d) Shape 17.

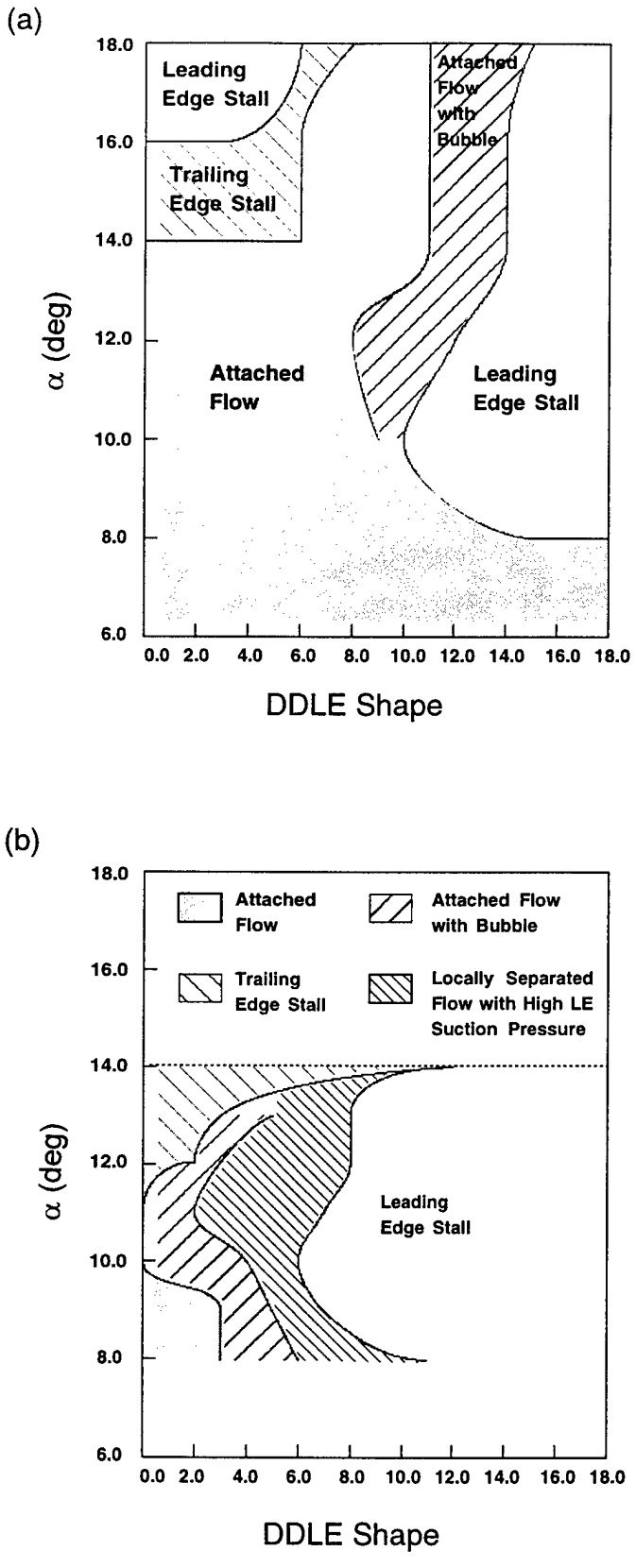

Fig. 21. Flow Regimes for Different Leading-Edge Shapes vs. Angle of Attack, k = 0.
(a) M = 0.3, (b) M = 0.45.

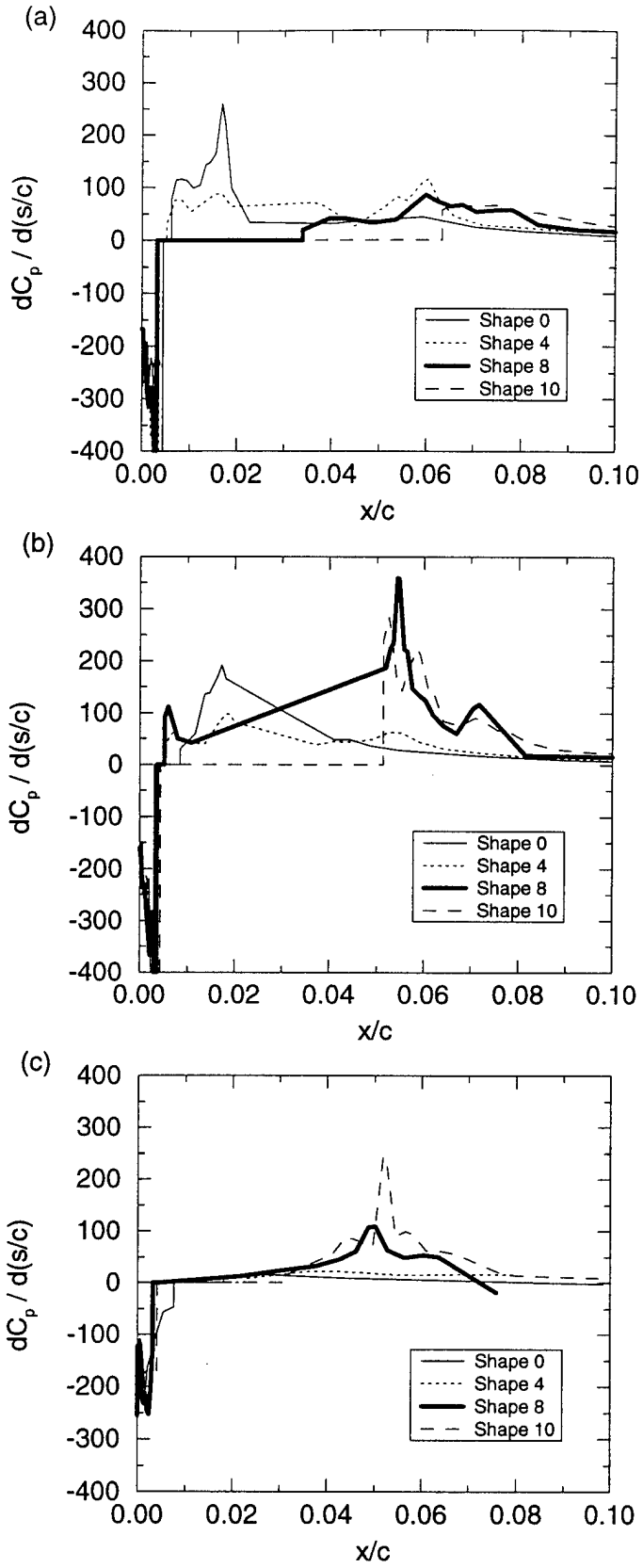

Fig. 22. Vorticity Flux Distributions for DDLE Shapes 0, 4, 8, and 10, M = 0.3, k = 0.
(a) $\alpha = 12.03^{\circ}$, (b) $\alpha = 13.99^{\circ}$, (c) $\alpha = 18.00^{\circ}$.

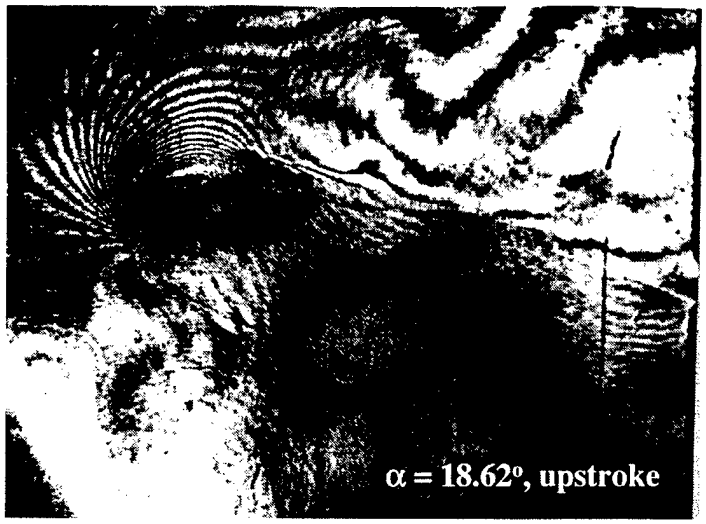

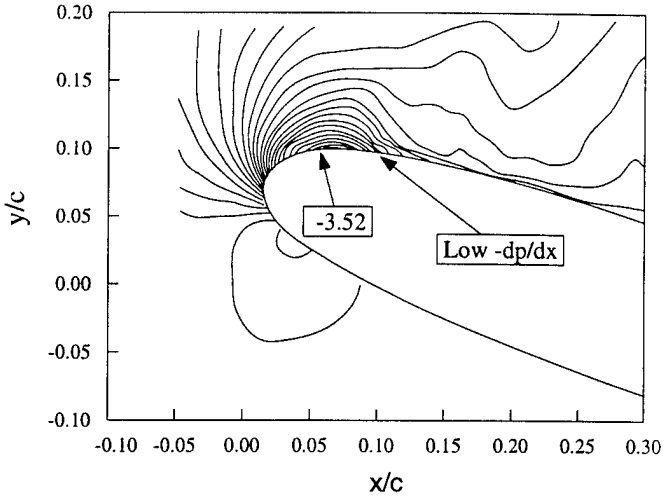

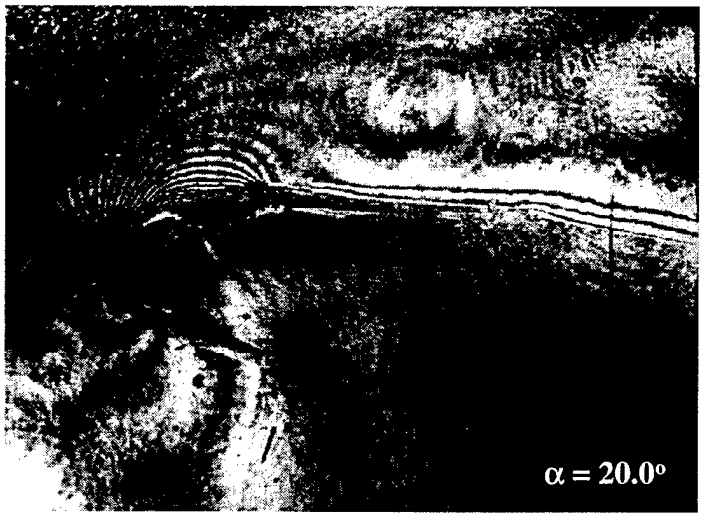

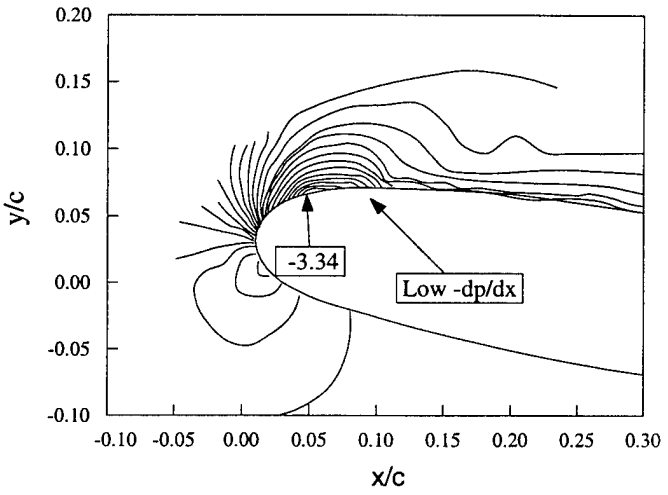

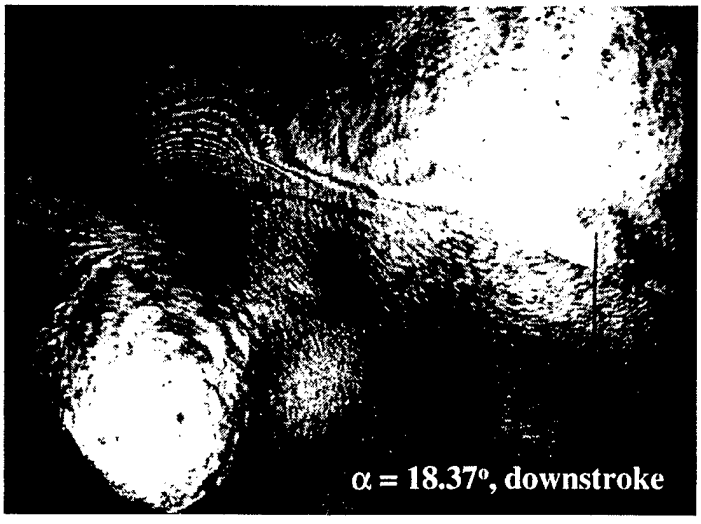

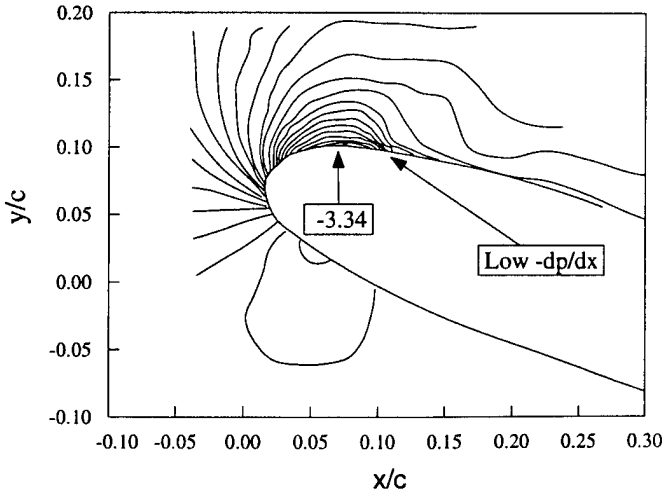

Fig. 23. PDI Images and Corresponding Global Pressure Distributions for Oscillating DDLE Shape 8 Airfoil, M = 0.3, k = 0.05, $\alpha = 10^{o} - 10^{o} \sin\omega t$.